Molecular Interactions for Physical Adsorption

William Steele

Department of Chemistry, 152 Davey Laboratory, Penn State University, University Park, Pennsylvania 16802

Received March 3, 1993 (Revised Manuscript Received July 8, 1993)

Contents

William Steele was born in St. Louis, MO, in 1930. He received a B.A. in chemistry from Wesleyan University (Connecticut) in 1951 and a Ph.D. in physical chemistry from the University of Washington in 1954. He held a post-doctoral position at Penn State under the direction of J. G. Aston for one year and joined the faculty there in 1955. He worked at Oxford University as an N.S.F. postdoctoral fellow in 1957–1958, at the University of Brussels as a senior post-doctoral fellow in 1963, as an Overseas Fellow at Churchill College (Cambridge) in 1971, as a Guggenheim Fellow at the University of Bristol in 1977, and as an Alexander von Humboldt senior fellow at the Technical University of Aachen in 1988. His research interests include studies of the properties of molecular liquids and physically adsorbed films by experiment and computer simulation. He served as an associate editor for the *Journal of Physical Chemistry* for nine years and is presently editor-in-chief of *Langmuir*.

1. Introduction

Modeling of the physical interactions of molecules with solid surfaces has been a subject of considerable interest for many years. These potentials play a central role in the theory and computer simulations of the thermodynamic, structural, and dynamic properties of adsorbed films.[1,2] Consequently, efforts are being made to devise accurate interaction laws for these systems. This review will be devoted to the physical interaction of simple molecules with solid surfaces and the relation between these energies and observable properties.

It should be stated at the outset that most potentials for molecule–solid interactions are still basically empirical. The ideas employed are often straightforward extensions of those which are widely used in the statistical mechanics and computer simulations of bulk liquids. The simplest versions of these model potentials are based on the idea that nonbonding interactions are pairwise additive to a good level of approximation, that they can be decomposed into electrostatic terms plus a dispersion–repulsion part, and finally, that the dispersion–repulsion parts for nonspherical molecules can be expressed as sums of spherically symmetric Site–Site energies which are generally written as inverse power-law functions. (These sites are capitalized below to distinguish them from adsorption sites which are defined later.) Thus it is often assumed that a pair of Sites α,β separated by a distance r_{SS} will have an interaction energy $u_{\alpha\beta}(r_{SS})$ given by

$$u_{\alpha\beta}(r_{SS}) = 4\epsilon_{\alpha\beta}\left(\left[\frac{\sigma_{\alpha\beta}}{r_{SS}}\right]^{12} - \left[\frac{\sigma_{\alpha\beta}}{r_{SS}}\right]^{6}\right) \quad (1)$$

with $\epsilon_{\alpha\beta}$ and $\sigma_{\alpha\beta}$ defined as the well depth and size for the pair of Sites. The total interaction for a pair of molecules 1 and 2 is a function of their separation r_{12} and their orientations, denoted here by Ω_1 and Ω_2. One can write

$$u(r_{12},\Omega_1,\Omega_2) = u_{elect}(r_{12},\Omega_1,\Omega_2) + \sum\sum u_{\alpha\beta}(r_{SS}) \quad (2)$$

where the double sum runs over all Sites in molecule 1 and in molecule 2. The electrostatic energy u_{elect} can be written as a sum over discrete charges distributed over each molecule or as a sum of ideal dipole–dipole, dipole–quadrupole, quadrupole–quadrupole, ... terms. (The charge distributions are normally adjusted to give the correct values of the known molecular multipole moments while maintaining a reasonable level of convenience.)

Let us consider how an interaction law of this kind can be adapted to deal with the problem of a molecule interacting with a solid adsorbent. As a first step,

0009-2665/93/0793-2355$12.00/0

assume that both the molecule and the solid are rigid. (Flexible adsorbed molecules such as normal hydrocarbons have been modeled—it is only necessary that the internal motions be well characterized.) The interaction energy $u_s(\mathbf{r},\Omega)$ for a molecule located at point $\mathbf{r}$ with orientation Ω is now written as the sum of an electrostatic interaction $u_{elect}(\mathbf{r},\Omega)$ and a dispersion–repulsion part $u_{SS}(\mathbf{r},\Omega)$:

$$u_s(\mathbf{r},\Omega) = u_{elect}(\mathbf{r},\Omega) + u_{SS}(\mathbf{r},\Omega) \quad (3)$$

where u_{SS} is a sum over the Sites in the adsorbate molecule and over the Sites in the solid adsorbent. Since the electrostatic energy is due to the molecular moments interacting with the charges or moments in the solid, a summation over these elements in the solid is also needed.

This brief description of the gas–solid interaction is hardly complete. Some suggested modifications and extensions will be discussed in section 5. Basic problems which must be dealt with if this model is to be applied to specific molecule–solid systems are: How does one parameterize realistic Site–Site interaction functions? How can one deal with the semiinfinite sums over the Sites in a macroscopic solid adsorbent? And how does one represent the resulting $u_s(\mathbf{r},\Omega)$ in a way which is computationally convenient and readily visualized?

Of the systems which have been modeled and tested against experiment, simple molecules interacting with the exposed basal plane of graphite form the largest group. It turns out that one can produce graphite with adequate specific surface area for experimental use which is chemically pure and stable and which presents surfaces that are almost entirely made up of large, nearly perfect pieces of exposed basal plane. From the theoretical point of view, this system has the advantage that one need sum over Sites of only one kind (C atoms) whose positions in the solid are precisely known. In fact, once the parameters of the Site–Site potentials have been estimated (see section 2), theory and/or computer simulations based on the resulting molecule–graphite interaction laws are generally found to be in good agreement with the existing body of experimental data. In section 4, the data for these systems which are most closely related to the molecular potentials will be discussed.

A widely used representation of the atom–graphite potential derives from the fact that one can approximate a finite exposed basal plane by an infinite, perfect two-dimensional single crystal. This approach, which is also applied to many other crystalline adsorbents, relies on the fact that the interaction at a fixed distance from the surface will have the same symmetry as that of the surface lattice. This allows one to express the variation in potential as a periodic function of the lateral position of the adsorbate molecule. These representations of the interactions will be discussed in detail in section 3, together with models of the interactions for atoms over solids which do not possess this surface symmetry.

One important class of solids which cannot be realistically treated by equations such as eq 3 is that of metals. In this case, the interactions with gaseous atoms or molecules are due in large part to the non-localized conduction electrons. Although there is a very large body of literature concerning adsorption on metals, most of it deals with chemisorption. The boundary between chemisorption and physisorption is particularly ill-defined for adsorption on metals. The usual distinguishing criteria are the magnitudes of the adsorption energy and the perturbations to the electronic wave functions of the solid and/or the adsorbate. Both criteria are qualitative rather than quantitative and the experimental data vary continuously from one extreme to the other. Another criterion which is sometimes invoked is that chemisorption can be an activated process, whereas physisorption is not. One consequence of this is that both chemisorption and physisorption can occur in the same system depending upon temperature, as has occasionally been observed in gas–metal systems. A discussion of gas–metal physisorption will be given in section 6.

2. Experimental Methods

2.1. Thermodynamics

A brief review[1] of the thermodynamics of physical adsorption should begin with the adsorption isotherm, which is an evaluation of the number of molecules adsorbed N_s as a function of the pressure or the concentration, for adsorption from liquid solution. In both cases, the equality of chemical potentials of the adsorbate on the surface and in the bulk means that an isotherm is essentially a measure of the chemical potential as a function of the amount of adsorbate on the surface, measured as an excess over the amount expected in the absence of adsorption. If one wishes to calculate the isotherm from a computer simulation,[2] one proceeds either by grand canonical Monte Carlo, where molecules are added and deleted at random as the simulation proceeds, or by the particle insertion technique.[3] In the latter case, a simulation of an N-particle system is carried out, and an extra particle is randomly added to the configurations generated; the average Boltzmann factor for such additions yields the chemical potential.

In addition to the isotherm, the coverage dependence of the isosteric heat of adsorption is often measured. This quantity yields the partial model enthalpy of the adsorbed material or, if the bulk gas is ideal, the partial molal average potential energy of adsorption. (It is also assumed here that classical statistical mechanics is applicable.) In simulations, it is straightforward to evaluate the average molal potential energy and a simple manipulation then yields the partial molal quantity.

In the limit of low density, expansions of thermodynamic properties in powers of the density become useful. Adsorption equations analogous to virial expansions of bulk gas properties are the result. (One can imagine the solid adsorbent as a single large "particle" in a grand canonical ensemble.) For an ideal gas in equilibrium with an adsorbed film, the result can be written as

$$p = N_s K_H^{-1} \exp[2B_{2D}(N_s/\mathcal{A}) + (3/2)C_{2D}(N_s/\mathcal{A})^2 + ...] \quad (4)$$

where B_{2D}, C_{2D}, etc. are virial coefficients for pairs, triplets, etc. of molecules near the surface, K_H is the

Henry's law constant, and $\mathcal{A}$ is the surface area of the adsorbent. One also has

$$q_{st}(N_s) = RT^2\{-(\partial \ln K_H/\partial T) + (2N_s/\mathcal{A})(\partial B_{2D}/\partial T) + (3/2)(N_s/\mathcal{A})^2(\partial C_{2D}/\partial T) + ...\} \quad (5)$$

for the isosteric heat of adsorption q_{st}. Furthermore, if classical statistical mechanics can be used to describe the adsorbed phase, the coefficients in eqs 4 and 5 are directly related to the potential energies of the molecules near the surface. In particular,

$$K_H = \frac{1}{WkT}\int\int_V (\exp[-u_s(\mathbf{r},\Omega)/k_BT] - 1)\, d\mathbf{r}\, d\Omega \quad (6)$$

where W is the normalizing factor for the integration over the adsorbate molecule orientation Ω and V is the volume available to the adsorbate. Also,

$$q_{st}(0) = RT + \frac{\int\int u_s(\mathbf{r},\Omega)\exp[-u_s(\mathbf{r},\Omega)/k_BT]\, d\mathbf{r}\, d\Omega}{\int\int (\exp[-u_s(\mathbf{r},\Omega)/k_BT] - 1)\, d\mathbf{r}\, d\Omega} \quad (7)$$

Of course, analysis of virial coefficient data for bulk gases is a standard technique for obtaining the parameters of molecular pair interactions. The analogous procedure applied to adsorbed gases involves comparison of the measured K_H and $q_{st}(0)$, the isosteric heat in the limit of zero coverage, with parameterized calculations of these quantities. This procedure becomes less useful when the solid surface is heterogeneous, since the gas–solid energy then becomes a complicated function depending upon the numerous parameters needed to properly describe heterogeneity. Comparisons of experimental and theoretical gas–solid virial coefficients including Henry's law constants began some time ago.[1] Data for rare gases and methane on the graphite basal plane have been fitted to calculated Henry's law constants and parameters of the gas–solid interaction laws have been evaluated.[4,5] Henry's law constants and second virial coefficients on graphite have been calculated and fitted to experiment for diatomics;[6-8] similar calculations for benzene[5,9] and for aromatic and saturated hydrocarbons[10] have been published. Quantum effects on the Henry's law constant[11-13] and on B_{2D}[14] have been considered. The evaluation of K_H and the second virial coefficient for heterogeneous surfaces has been discussed;[1,15-18] the second surface virial coefficient has also been treated for Ar on graphite[19] and for model gases on a structureless surface.[20]

In the case of B_{2D}, the theoretical expressions contain integrals over the positions of pairs of molecules in the neighborhood of the surface and thus are sensitive to the adsorbate–adsorbate pair potential as well as the adsorbate–solid potential. Fits of theory and experiment can produce information concerning pair potentials for molecules in the vicinity of the solid, but the calculation is a difficult one except for the simplest gas–solid systems and consequently has not yielded much useful information to date.

Finally, the general virial expansion for fluids in an external potential field, with applications to sorption in zeolites, has recently been reexamined.[21] Calculations of virial coefficients for systems with explicitly periodic gas–solid interactions have also been given.[22,23]

Table I. Bound-State Energies for Helium on Graphite

	energy per k_B (K)			
level n	ref 25	ref 27	ref 28	ref 29
0		−139	−144	−142
1	−75	−73	−76	−76
2	−34	−33	−35	−36
3	−13	−11	−14	−14
4	−3	−2	−5	−6
5			−2	−2

2.2. Beam Scattering

Modern experiments on the nonreactive scattering of molecular beams from well-characterized surfaces are capable of producing considerable information about the interactions of the beam molecules with surfaces.[24-26] Although there is an analogy between these experiments and beam–beam scattering in the gas phase, the beam–surface problem has several complicating factors which are not a significant part of the interpretation of crossed-beam data. In the surface case, one must take inelasticity in the gas atom–surface collisions into consideration. Also, most data are interpreted in terms of the quantum description of scattering, which limits the gases involved to helium and hydrogen. Finally, if the surface is regular but strongly corrugated, the scattering calculations become rather complex. Particularly successful experiments of this kind have been helium beam scattering from the exposed graphite basal plane, from single-crystal metal surfaces, and from the (100) face of LiF, although helium from other alkali halide crystal faces has also received considerable attention. Two popular types of observation have been diffraction and resonant capture by selective adsorption of beam atoms into surface bound states. Of course, the diffracted beam directions are dependent upon the symmetry and lattice size of the surface crystal; the intensity of the diffraction depends upon the amplitude of the surface corrugation. In the case of selective adsorption, direct measurements of the energy levels for an adsorbed atom can be obtained. As a specific example, data for the helium–graphite basal plane system have been reported by several groups.[25] Measured diffraction intensities can be quantitatively fitted to a corrugated hard-wall model with the correct symmetry and spacing for graphite, and values of 0.21 and 0.15 Å have been obtained for the amplitude of the surface corrugation by separate groups using different graphite samples. In addition, the bound-state energy levels for helium on graphite have been evaluated from selective adsorption experiments. The results are summarized in Table I and exhibit quantitative consistency from one study to another. When combined with similar but less extensive results for ^{3}He on graphite, the level schemes can be fitted to a potential function which gives a He–graphite adsorption surface-averaged well depth of $u_{ads}/k_B = 175$ K (±10%) and an energy corrugation per k_B of 3.3 K.

In the quantum limit, the heat of adsorption at zero coverage is written as a sum over the energy states of an isolated adsorbed atom times a Boltzmann probability weighting factor. For a light rare gas on graphite, the periodicity of the potential causes the surface-averaged levels to spread into bands, which complicates the sum over states. Helium–graphite potentials and the associated band structure of the surface energy have

been considered by several authors[12,30,31] and calculations of the heat of adsorption have been reported. Values for the average energy E_{ave} for an isolated adsorbed helium atom can be calculated from the experimental $q_{st}(0)$ since $E_{ave} = 2.5RT - q_{st}(0)$. Estimates of this energy per R at 15 K are in the range −122 to −144 for ^{4}He and −133 for ^{3}He,[12] and, by extrapolation, −142 and −136 for the two isotopes at 0 K. The 0 K results are completely consistent with calculated energies based on the surfaced-averaged levels obtained from the scattering experiments and the associated band structure obtained from the assumed periodicity.[31] This comparison is thus a test of the accuracy of the assumed periodicity of the potential, in contrast to the earlier calculations in which a model for the entire potential function was developed. These are not nearly so precise, giving heats at 20 K which differ from experiment by roughly 20%.

2.3. Diffraction from Overlayers, Atomic Microscopy, Spectroscopy

Experiments which have greatly altered our understanding of the behavior of molecules in monolayers at low temperatures are determinations of diffraction from the overlayer itself. With some effort, this can be done with helium beams; the older and, in some ways, easier technique is low energy electron diffraction (LEED).[32] Both neutron[33-35] and X-ray[35,36] diffraction have been shown to be powerful methods for the study of overlayer structure. Although the determination of molecular orientation on the surface by these techniques is difficult, the evaluation of two-dimensional unit cell size and symmetry has become almost routine. These measurements thus provide crucial data for the elucidation of the interactions of the molecules in the monolayer with the underlying solid and with their neighbors in the overlayer. Specific examples of such studies of monolayers on graphite will be discussed in section 4.

Of course, diffraction measurements provide information about molecular positions in the adsorbed layer for a rather small class of systems where the surface is sufficiently perfect and the temperature sufficiently low to produce a two-dimensional crystal with long-range order. Other techniques are needed to locate adsorbed molecules when the adsorbate has only short-range order (or none at all, especially on certain heterogeneous surfaces). Techniques which can at least potentially provide such information are scanning tunneling microscopy (STM) and atomic force microscopy (AFM).[37] The resolving power of these microscopes is in the subangstrom range, and the systems that can be studied seem to be unlimited. As an example, the adsorption of xenon on a stepped platinum surface has been followed by STM.[38] After the initial adsorption at the step, addition of more xenon to the surface at low temperature causes the layer to grow by addition to the previously adsorbed atoms to form patches that gradually cover the terraces between steps. Similar behavior is seen if the metal surface possesses a defect which is the initial adsorption site. As the xenon coverage increases, a two-dimensional cluster forms around the atoms initially adsorbed at the defect.[39] Reports of the use of AFM to study the surface roughness of nonconducting solids are now beginning to appear. These include measurements on an activated carbon black,[40] on mica and clay,[41] and on a zeolite.[42]

It has long been known that adsorbate spectra can be used in several ways to characterize molecular interactions with a surface. The most obvious of these has to do with chemisorption, since one ordinarily associates this with significant alterations in the electronic structure of the adsorbate molecules which then produce changes in electronic and vibrational spectra when a molecule is adsorbed. However, there can be interesting spectral changes in the infrared spectrum even in the case of physisorption: if molecular rotation is hindered on the surface, infrared bands will be narrowed relative to the gas phase; interactions with the surface can produce vibrational frequency shifts; and the presence of an electric field at the surface of the solid can alter spectral intensities, including the induction of spectral bands in normally nonpolar molecules on ionic solids. There is extensive literature in this area. Here, we discuss only a few recent examples of such studies.

Infrared spectra of the isotopes of hydrogen[43] and methane[44] adsorbed on the NaCl(100) surface have been reported in which both the band shapes and the intensities were measured as a function of the amount of gas on the surface. The integrated intensity σ due to the electric field at the surface of a solid has been written as

$$\sigma = \frac{1}{12\epsilon_0 \mu c^2} E_z^2 \left(\frac{d\alpha_\perp}{dr}\right)^2 \qquad (8)$$

where μ is the reduced mass of the (diatomic) molecule, $4\pi\epsilon_0 = 1.1 \times 10^{-10}$ J^{-1} C^2 m^{-1}, E_z is the electric field perpendicular to the surface at the molecule, and the derivative is the change in the molecular polarizability with the stretching coordinate r (perpendicular to the surface). In the hydrogen case, the spectra are completely due to this induction. The spectra for this molecule on NaCl actually show six vibration–rotation bands spread over a 100-cm^{-1} range. The dependence of the band intensities on surface coverage leads to the conclusion that three bands are due to adsorption on the flat parts of the (100) plane and the other three are due to defect sites of some kind which fill first as the gas is adsorbed at ~30 K. The quantitative intensity measurements allow one to estimate the magnitude of E_z, and from this and the calculated field for the flat region of NaCl(100), one can estimate the distance between the adsorbed molecules and the surface. It was also observed that the magnitudes of E_z associated with the defect sites are six times larger than those for the flat surface. The three bands of each kind can be interpreted as, first, a pair of vibration–rotation transitions and, second, a combination of the vibrational modes perpendicular and parallel to the surface.

In the case of methane adsorbed on NaCl and KCl,[44-46] the surface electric field can induce absorption for the ν_1 inactive mode as well as causing splittings in the active 3-fold degenerate ν_3 and ν_4 modes. This lifting of the degeneracy has also been observed for methane in a zeolite and is associated with a low-symmetry environment for the adsorbed molecules; i.e., a crystal field splitting.[47] Use of incident radiation polarized parallel and perpendicular to the single-crystal surface allows one to deduce the directions of the transition

dipoles in the split spectra and leads to the conclusion that these molecules are not rotating on the surface at 42 K but are either tripod- or dipod-down. Indeed, the use of polarized incident radiation on single-crystal surfaces is a powerful technique which has been applied to other systems such as CO on NaCl(100) to determine the orientation of the adsorbed molecules—see below. The infrared spectra of carbon dioxide on NaCl(100) and carbon monoxide on MgO(100) will also be discussed in section 3.3 in connection with work on the potential functions and the monolayer unit cells on these surfaces.

Spectra have also been reported for CO_2[48-50] physisorbed on the (100) face of MgO. CO_2 also chemisorbs on this surface.[51] Of course, chemisorption will produce major changes in the infrared frequencies associated with the CO_2 moiety. An *ab initio* calculation of the interactions of CO_2 with MgO has been reported[52] and the results have been compared with the spectral data for this system. The conclusion drawn from both experiment and theory is that both types of adsorption can occur simultaneously. The calculations indicate that CO_2 orientations perpendicular to the surface are slightly preferred to those which are parallel. The observation of the infrared-forbidden ν_1 symmetric stretching mode in the adsorbed CO_2[49] indicates that these molecules are indeed perpendicular to the surface and distorted by the electrostatic field of the solid.

Other recent studies of infrared spectra include hydrogen physisorbed on porous glass, silica, and MgO[53] and CO on hydroxylated silica.[54]

3. Molecule–Solid Potentials

3.1. General Aspects

Consider first the interaction of a monatomic gas with a solid that is approximated as an infinite single crystal.[55-58] The potential will possess a two-dimensional periodicity which is produced by and thus is identical to the periodicity of the exposed surface. One defines a surface unit cell by a pair of two dimensional vectors $\mathbf{a}_1,\mathbf{a}_2$. The unit cell is thus a rhombus which, when translated by integer multiples of $\mathbf{a}_1,\mathbf{a}_2$, generates the surface crystal. Reciprocal lattice vectors $\mathbf{b}_1,\mathbf{b}_2$ are defined such that

$$\mathbf{a}_1\cdot\mathbf{b}_1 = \mathbf{a}_2\cdot\mathbf{b}_2 = 1 \tag{9}$$

$$\mathbf{a}_1\cdot\mathbf{b}_2 = \mathbf{a}_2\cdot\mathbf{b}_1 = 0 \tag{10}$$

The periodicity of the atom–solid potential can now be explicitly shown by writing

$$u_s(\mathbf{r}) = \sum_\alpha \sum_{\mathbf{g}} u_{\mathbf{g}}(z_\alpha) e^{i\mathbf{g}\cdot\tau} \tag{11}$$

where $\mathbf{r} = z,\tau$ with z equal to the distance between the gas atom and the surface plane and τ denoting its position in the plane. The two-dimensional vector $\mathbf{g} = n_1\mathbf{b}_1 + n_2\mathbf{b}_2$, with n_1,n_2 equal to integers. The summation over α is over the stack of planes in the solid parallel to the surface at distances z_α from the gas atom.

The series expansion of eq 11 is only of use if it converges rapidly and if the coefficients $u_{\mathbf{g}}(z_\alpha)$ can be conveniently evaluated. In fact, an equation of this form was used over 60 years ago in a calculation of the electrostatic potential near the surface of an ionic crystal.[59] For Coulombic interactions, the form of $u_{\mathbf{g}}(z_\alpha)$ is actually a simple exponential function of z_α. In general, one evaluates the coefficients from

$$u_{\mathbf{g}}(z_\alpha) = \frac{1}{a_s}\int e^{-i\mathbf{g}\cdot\tau} u_s(z_\alpha,\tau)\, d\tau \tag{12}$$

where a_s is the area of the surface unit cell. If $u_s(z_\alpha,\tau)$ is written as a sum over Sites in the αth layer, and t is defined by $\tau - \mathrm{m}_k - \mathbf{l}$ ($\mathbf{l}$ being a vector denoting the position of a unit cell in the surface), one finds

$$u_{\mathbf{g}}(z_\alpha) = \frac{2\pi}{a_s}\sum_k e^{i\mathbf{g}\cdot\mathbf{m}_k}\int_0^\infty J_0(gt)u_{gk}(\rho)t\, dt \tag{13}$$

where $u_{gk}(\rho)$ is the interaction of the gas atom with the kth type of Site, and m_k is the location of one of those Sites in the cell. The atom–Site separation distance $\rho = (z_\alpha^2 + t^2)^{1/2}$. The integral involving the Bessel function J_0 can be evaluated analytically for u_{gk} which are inverse power law functions,[55] so that the coefficients $u_{\mathbf{g}}(z_\alpha)$ are often reasonably easy to calculate. Also, for many single-crystal surface planes, the number of atoms (or Sites) per unit cell is small (2 for the graphite basal plane, 2 for the low order Miller planes of alkali halide crystals, 1 for the low order Miller planes of many metals, etc.).

As one varies n_1,n_2, the values of the vector $\mathbf{g}$ actually define the entire reciprocal lattice. Consequently, the number of $\mathbf{g}$ values for a given length g depend upon the symmetry of the lattice. For the graphite basal plane, one has six values for the smallest nonzero $g = 4\pi a/\sqrt{3}$, where a = unit cell edge length = 2.46 Å. These correspond to $n_1,n_2 = \pm1,0;\ 0,\pm1;\ +1,+1;\ -1,-1$. It emerges that the nonperiodic term plus those for these six nonzero $\mathbf{g}$ values gives an adequate representation of the gas–graphite interaction for all gases of interest to date. For many purposes, it is even possible to omit all the periodically varying terms in this molecule–solid potential.

Another feature of this expansion is that terms with $g \neq 0$ decay very rapidly with increasing z, so that contributions from planes with $\alpha > 1$ ordinarily do not contribute to this part of the interaction. Even the terms with $g = 0$ decay rapidly, for an inverse (12,6) power law atom–Site energy. Consequently, one obtains accurate surface-average energies in the region near the minimum by either cutting off the series in α after one or two planes beyond the surface plane or by using simple approximations to sum the series to infinity.[4] The leading $g = 0$ term expresses the energy obtained by smearing out the atomic structure in the surface and interior planes into continua. For a single plane, the smearing of the inverse (12,6) power law interaction produces an interaction which varies as the inverse (10,4) powers of z_α; the summation over α gives an asymptotic long-range form which varies as z^{-3}. The periodically varying part of the potential is due almost entirely to the atomic structure of the outermost layer of the solid. The only significant exceptions to this are interactions with some Miller plane surfaces of ionic crystals where a summation of Coulomb energies necessitates inclusion of more than one layer of ions to accurately evaluate the periodic terms. In general, the magnitude of the periodicity in the interaction potential relative to the nonperiodic part depends very much upon the relative sizes of the gas atom and the surface Sites.

Evaluation of the nonperiodic part of the interaction potential for single-crystal surfaces or for surfaces where heterogeneity plays a minor role is an important first step in characterizing the molecule–solid interaction. Considerable effort has been expended on this problem over the years and the results have been critically reviewed recently.[60] A somewhat more limited review of the information concerning the long-range asymptotic behavior of the potentials which are obtained from beam scattering experiments has also appeared.[24]

Theoretical or computer simulation studies of physical adsorption on nonperiodic or perfectly flat surfaces have been popular for many years.[2] While this work has led to useful physical insights concerning the structure of fluids near surfaces and in pores, it obviously has its limitations. One learns nothing about the effects of surface structure upon the formation and growth of ordered (i.e., solidlike) films. Unexpected structural and thermodynamic features have been observed which are a consequence of the periodicity of the surface (see below). Another defect of the perfectly flat surface models is an inability to properly model flow in pores, since a featureless pore wall will give only slip flow unless some arbitrary condition is applied to prevent the molecules from sliding freely along the walls. Not surprisingly, models of slit pores which are single-crystal lattice planes give much more realistic flow properties than those with slip boundary conditions.[61-71] However, it becomes increasingly difficult to model the walls of cylindrical pores by crystalline surfaces and this difficulty obviously extends to other nonplanar surface geometries. Thus, it is important to consider how one might model surfaces for which the atomic structure is explicitly present, but not as an exposed single-crystal plane. Of course surfaces which contain symmetry-breaking defects, either physical or chemical, are the rule rather than the exception in systems of practical interest. The presence of steps[72,73] or cracks would be expected to produce rather large local changes in the atom–surface interaction. Similarly, the presence of chemical impurities in an otherwise perfect lattice can also produce large changes in the potential which will depend upon the nature, the number and the spatial distribution of the defects. A typical case is produced by the partial oxidation of a nonpolar solid such as carbon black. It is generally believed that the gas–solid potential for a polar molecules over oxidized carbon black is very different from that for the clean or unreacted surface. If the oxidation occurs preferentially at the basal plane edges, as is likely to be the case, polar impurities will be concentrated in particular regions rather than scattered randomly over the surface. It is also believed that the properties of a film adsorbed on such a surface will be sensitive to the spatial distribution of the impurity Sites.

Two questions arise at this point: how can the adsorption potential $u_s(z,\tau)$ be calculated for an imperfect surface, and how can the results be presented? Current computer power is such that it is no real problem to directly sum atom–Site energies over the solid, for many kinds of physical roughness or the chemical heterogeneity. In practice, accurate energies are obtained for (12,6) inverse power law atom–Site interactions if one sums over the nearest several hundred Sites in the solid. A correction term for more distant Sites can be evaluated by replacing the discrete atomic structure by a continuum and integrating over this region. However, the numerical tabulations of the large arrays of numbers generated in this way for the three-dimensional $u_s(z,\tau)$ are not easy to use nor are they very enlightening. In this respect, one can make some progress by considering the minimum energies $u_{ads}(\tau)$ as a function of location over the surface. Since adsorbed species are usually located at or near these minima, they are the local adsorption energies. (Note that thermodynamic adsorption energies contain contributions from the adsorbate–adsorbate interactions as well as the gas–solid interactions.) Their variation with τ contain local minima that are sites for localized adsorption, when it occurs. The adsorption site is unfortunately not the same as the Site in the atom–Site pairwise interaction model. For clarity, the word has been capitalized in this article when referring to the interaction Site model. Also, the barriers to translation across the surface which are believed to determine surface diffusion are obtainable from $u_{ads}(\tau)$.

A heterogeneous surface which can be modeled without too much difficulty is that for an amorphous material such as the high specific surface area solids often encountered in practical applications. Of course, a variety of surface defects may be present in these adsorbents, but modeling the nominally planar surface is at least a first step in producing a realistic description. Since many of these materials are oxides such as silica, titania, or alumina, we can consider a mostly covalently bonded oxide for which the adsorption energy may be approximated by the dispersion–repulsion interactions of the gas atoms with the oxides. Coulombic terms are often omitted as are the interactions with the metals. The latter omission is justified on the grounds that the oxides have considerably greater polarizabilities than the metals in these solids and thus should have much larger dispersion interactions. A calculation of adsorption energy is based upon an algorithm[74] for building a block of hard spheres with random close packing. The computer program for this purpose was originally developed in connection with studies of amorphous metals and embodies periodic boundary conditions in two dimensions (at least). Thus, one can generate a cube of roughly 1000 spheres with exposed amorphous surfaces each containing roughly 100 spheres. Due to the periodic boundary conditions, the surface can be replicated to infinity in the directions parallel to itself. (This algorithm is a realization of the physical model of a liquid studied by Bernal in the 1930s by randomly filling a box with spheres and then counting coordination numbers, spatial distributions of neighbors and so on.) The "Bernal" model can be readily transformed into an amorphous adsorbing solid by associating an interaction Site with each sphere.[75-78] Other similar models have been used to describe adsorption on amorphous materials, especially silica.[79-82] One feature of these potentials is that the basic ideas can be readily adapted to complicated geometries, such as spherical particles in a packed powder or microporous sorbents. In fact, the Bernal solid provides a starting point for a wide range of adsorbents, since chemical heterogeneities can be introduced by altering the well depth, the size, and, if necessary, the charge on an

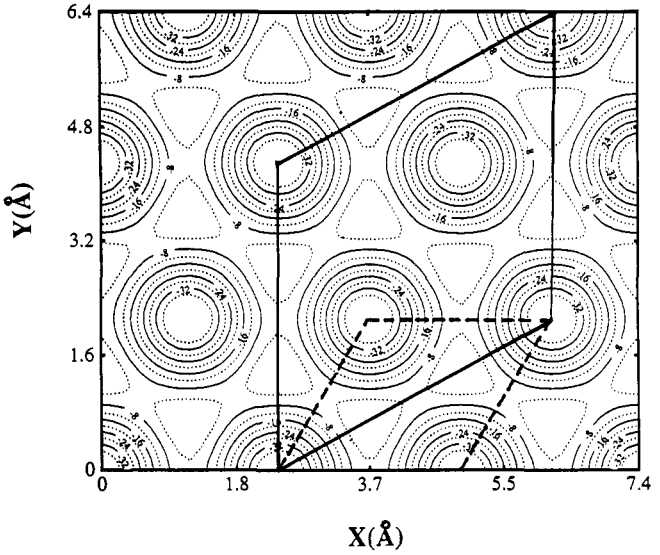

Figure 1. Contours of constant adsorption energy for a krypton atom over the basal plane of graphite. Contour lines are drawn for changes of 40 J/mol in adsorption energy, calculated relative to the points of weakest adsorption. These are located directly over the C atoms, which are at the centers of the dotted triangular regions. The deepest wells occur over the centers of the C hexagons, where the energies are −12 270 J/mol. The two rhombuses show unit cells for the graphite lattice (dashed lines) and for a commensurate $\sqrt{3} \times \sqrt{3}$ overlayer lattice (solid lines). Note that the numbers on the curves are energy (in J/mol) × 0.1.

arbitrary number of spheres at or near the surface of the original model. Furthermore, the spatial distribution of the chemical heterogeneities can be varied from random to patchwise, with many intermediate possibilities as well. Various kinds of physical imperfection can be introduced merely by deleting unwanted atoms: the surface can be roughened by random removal of surface atoms; pits or cracks of various sizes and shapes can be created; and pores of an arbitrary geometry can be produced. For example, cylindrical pores with constrictions are among the interesting pore shapes which can now be studied by computer simulation.[83] Work on such systems in presently in a very early stage.

3.2. Adsorption Energy for Kr on Graphite

The differences in the various model gas–solid systems can be illustrated by showing adsorption potential energy diagrams for a few representative cases. We begin by considering the energy variations for a krypton atom over a graphite basal plane.[55,84] Parameters for the Kr–C Site energy (and a number of other gas–C Site energies) have been evaluated from the Henry's law data for gases adsorbed by graphitized carbon black.[4,60] Although the analysis of this data gives reasonably reliable information about the surface-averaged nonperiodic part of the potential, the information concerning the periodicity obtainable from measurements of Henry's law constants is somewhat questionable (see section 4). In any case, the Kr–C Site energies can either be directly summed or written in terms of the Fourier expansion of section 3.1—the results are essentially identical. Figure 1 shows the calculated contours of constant energy (in units of joule/mole) of $u_{ads}(\tau)$ for the Kr–graphite system. The energy difference between adjacent contour lines is small, amounting to 40 J/mol out of a total surface-averaged adsorption energy of −11 840 J/mol. Thus, this surface is relatively flat as far as the periodic variation in adsorption energy goes. This weak variation in energy does significantly affect the structure of the Kr monolayer on graphite, since it plays a major role in producing a commensurate lattice in which the Kr atoms lie over carbon hexagons, presumably at their centers. Such a lattice built on occupation of second neighbor hexagons yields a two-dimensional crystal in which $^1/_3$ of the hexagons are covered, and which has a unit cell rotated by 30° relative to that of the underlying graphite lattice. The C atoms of the graphite surface are not shown in Figure 1, but lie at the midpoints of the triangles formed by the lattice of Kr adsorption sites. These sites are wells which are only 430 J/mol deeper than the energy at the weakest points, which are directly over C atoms. Unit cells for the graphite lattice and for the commensurate Kr monolayer are shown in the figure by the dashed and the solid lines, respectively. These unit cell edge lengths are 2.46 and 4.26 Å for graphite and commensurate Kr, respectively, compared to the Kr size σ = 3.60 Å or r_{min} = 4.04 Å, where r_{min} is the separation at the minimum of the Kr–Kr interaction. It is evident that the Kr atoms are slightly undersized for a perfect fit in the commensurate lattice where the intermolecular spacing is 4.26 Å. However, the small potential wells associated with the adsorption sites on this surface are sufficient to stabilize this lattice structure in preference to the natural two-dimensional crystal. The same commensurate lattice has been observed for a number of other simple gases on graphite including (r_{min} values are given in parentheses): He (2.87 Å); H_2, D_2 (3.29 Å); CH_4 (4.28 Å); N_2 (4.15 Å); and Xe (4.60 Å). significant quantum effects for helium and hydrogen produce lattices which are expanded relative to the expected "classical" size. In other cases, there is a good match of r_{min} and the commensurate lattice size, with the possible exception of xenon. In this last case, the data indicate that the commensurate lattice will form even when there is size mismatch if the corrugation in the gas–solid potential is sufficiently large and the temperature is sufficiently low.[85] In fact, it should be noted at this point that evidence has been accumulating that the periodicities on graphite given by the pairwise sum of spherical atom–Site functions are too small by roughly 50%. A possible reason for this and some of the experimental evidence for it are discussed below.

Another way to view a surface is to evaluate the physical roughness exhibited for a particular adsorbing gas. This roughness clearly depends upon the size of the probe atom, a fact which plays a role in current fractal descriptions of surfaces.[86,87] One can define surface roughness in different ways, but a convenient choice is based on an evaluation of the position of the minimum in the gas–solid energy (i.e., the adsorption energy) as an atom moves across the surface. For example, contour lines for the position of the minimum in the gas–solid potential are shown in Figure 2 for the Kr–graphite system. These lines follow the energy contours of Figure 1, as expected. The corrugation, which might be used in an interpretation of Kr-surface atomic beam diffraction (if the atoms were light enough

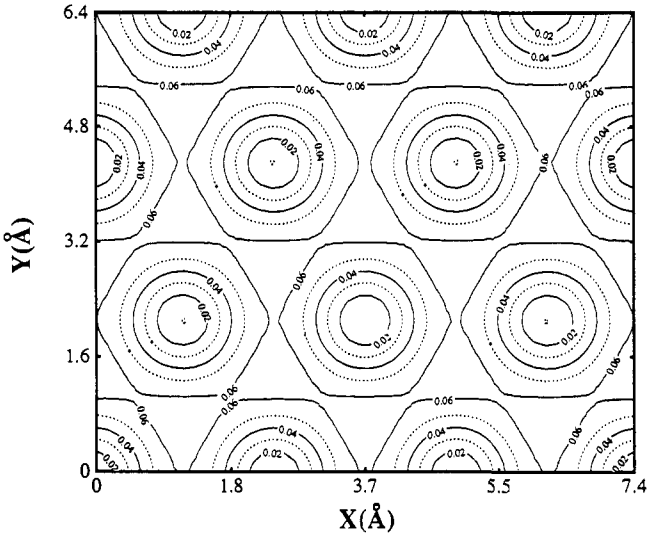

Figure 2. Contours of constant well-depth position for the curves of Kr–graphite energy. Contour lines are drawn for changes of 0.01 Å, calculated relative to the lowest points on the surface, which occur over C hexagon centers. The total difference between the highest and the lowest points amounts to 0.06 Å with the highest points occurring over the C atoms.

to be diffracted) is directly obtainable from Figure 2, since it is defined as the difference between the highest and the lowest points on a periodic surface. In the present case, this amounts to only 0.06 Å. Note that this corrugation strongly depends upon the energy value chosen for the calculation. If one were to choose an energy which is positive (and thus repulsive), the corrugation will be larger than that obtained using the minimum energy. Conversely, the corrugation becomes very small for energies corresponding to an atom at a large distance from the surface. (This choice is particularly relevant to beam scattering, where the "penetration" distance obviously depends upon the incoming beam velocity perpendicular to the surface.)

Contour diagrams such as that shown in Figure 1 have long been used to present the variations in adsorption energy over single crystal surfaces. Early calculations were carried out[88] for various rare gases on the (100) and (111) facs of a solid xenon crystal. This is of course a particularly favorable case for the pairwise Site interaction model, especially since the parameters of the potentials are relatively well known. The contour diagrams for these systems show adsorption sites located directly over the centers of squares or triangles of surface xenon atoms, saddle points in the energy located above the midpoints between pairs of xenon atoms, and points of weakest adsorption located directly above surface xenon atoms.

3.3. Adsorption Energy for Gases on Ionic Crystals

There is a long history of calculations of adsorption potentials for simple gases adsorbed on the exposed low index Miller planes of ionic crystals, especially alkali halides.[23,59,89-101] Although the electrostatic potential near the surface of an ionic crystal of known surface morphology is readily evaluated, estimation of the constants in the dispersion–repulsion part of the interaction are still subject to some uncertainty. Nevertheless, explicit energy contours have been evaluated for several rare gases over the exposed (100) surface planes of selected alkali halides.[23,97] An interesting aspect of this calculation is the effect of surface relaxation upon the gas–solid potentials.[23] That is, atomic positions near the surface of a crystalline solid are known to shift somewhat from those expected for the truncation of a perfectly rigid solid. The calculations indicate that this relaxation can noticeably alter the energy of adsorption on the NaCl(100) surface—by 6% for Ar, 20% for H_2, and 25% for N_2. Note that there are considerable quadrupole interactions with the electrostatic field gradients near the surface in the cases of H_2 and N_2.

The extensive studies of helium beam scattering from alkali halides have led to considerable efforts to evaluate gas–solid potentials for these systems. The experimental results have recently been reviewed.[102] Intensities of the diffracted beams can be interpreted in terms of a surface corrugation which is consistent with the known ionic radii. Measurements of selective adsorption have yielded precise surface-averaged potentials for these systems.[60,102] Calculations of the summed two-body interactions have been reported for the He–LiF and the He–NaCl[103] interaction. The ideas developed in these papers were later applied to He–NaF and He–LiCl.[104] In these studies, the He–ion interactions were adjusted to give agreement between the calculated and the experimental surface-averaged energies. Values found for the minimum in this energy per k_B for helium amounted to −97 K on LiF, −90 K on NaF (this shows that a change in the cation is not significant compared to the nearly constant $He–F^-$ energy, as one might expect), and −71 K on NaCl. Conceivably, such calculations could be extended to other nonconducting solids where one is reasonably confident that separate ions have distinct identities from a quantum mechanical point of view. However, as usual in such problems, the difficulty of an *a priori* computation increases very rapidly as the number of electrons in each of the interacting species increases.

Energy contour lines for Ar on the unrelaxed (100) faces of NaCl and KCl are shown in Figure 3. Although the preferred site for Ar adsorption is directly over the Na^+ ion for NaCl, the site has shifted to a point centered over a square of ions for KCl. Note that the Ar–ion interaction curves have been chosen to be essentially identical for the K^+ and the Cl^- but the well depth for the $Ar–Na^+$ interaction is roughly $^1/_8$ that for either of the other ions. Consequently, the adsorption site on KCl minimizes the energy of interaction with any four ions in a unit cell, whereas on NaCl the sites are such as to minimize the interaction with four chloride ions. In these calculations, the energy due to the interaction of the dipole induced in the rare gas atom by the electrostatic field with the field makes up a significant part of the total. The magnitude of this induction energy is proportional to polarizability times the square of the field and thus decreases quickly with increasing distance from the surface due to the exponential decay of the field. Indeed, it has been suggested[105] that the gradients of the electrostatic fields near the surfaces of ionic crystals are sufficiently large to give a nonnegligible energy when they couple with the next higher order polarizability (quadrupolar) in an adsorbate molecule.

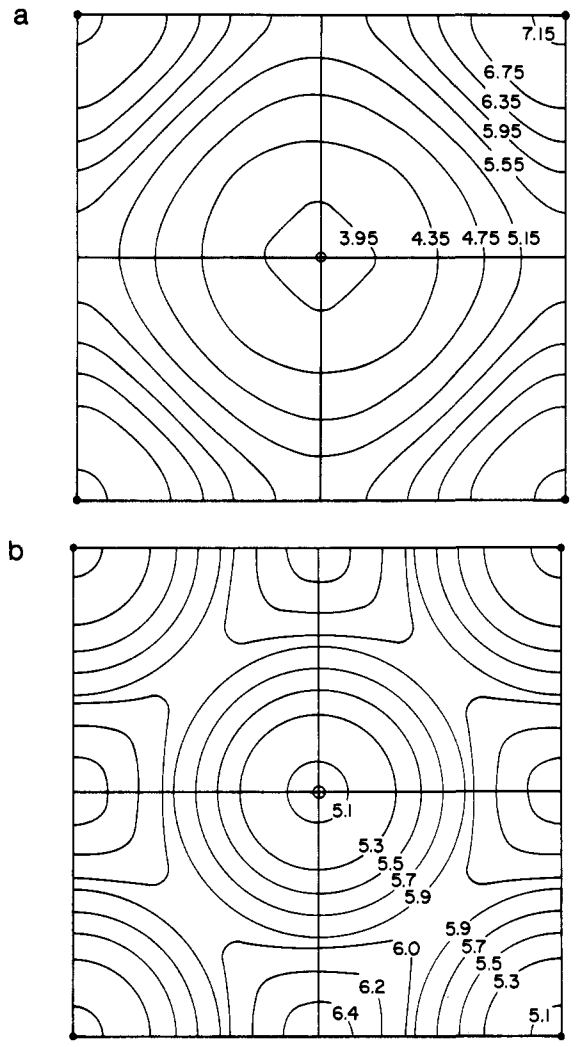

Figure 3. Contours of constant adsorption energy for an argon atom over the (100) faces of a NaCl crystal (part a) and a KCl crystal (part b). Values of the adsorption energy for each contour in kJ/mol are shown on the contour. In each case, the anion is located at the center of the figure, with cations at the corners (from ref 97).

Although the presence of these calculated sites for adsorption on the alkali halide surfaces would favor the formation of commensurate overlayers, it should be remembered that a commensurate layer on the (100) face would be expected to have square symmetry and thus only four nearest-neighbors compared to six in the close-packed incommensurate hexagonal lattice. Thus, a detailed calculation is necessary to determine which ordered lattice will actually be favored for a given gas–alkali halide pair. For example, experiment has shown that the xenon monolayer on the (100) surface of NaCl is incommensurate hexagonal, with two domains which differ in their orientation relative to the substrate.[106] Very recently, another study of this system has appeared[295] in which the earlier results were confirmed and extended using LEED to determine the lattice parameters.

The orientational behavior of polar molecules on the surface of a salt crystal is also a competitive situation. The Site–Site model predicts that the favorable orientation will usually be one with the maximum number of gas molecule Sites in contact with the surface. However, the alignment of dipole or quadrupole moments in the electrostatic field at the surface is often favorable when the electrostatic moment is perpendicular to the surface. For example, a linear molecule will lie flat on the surface in the absence of electrostatic interactions, but will orient perpendicular to the surface when the latter interaction is dominant. When interactions with the neighboring adsorbate molecules in a dense monolayer are included, it is quite possible that the favored orientation will be altered from that expected for isolated molecules on these surfaces.

Recently the interactions of methyl bromide and iodide with (100) face of LiF have been calculated.[10] Although these molecules are predicted to lie parallel to the surface at low coverage, the energy of the monolayers are minimized when the molecular axes are perpendicular to the surface with alternating directions of the dipole moments. (In the case of methyl bromide on NaCl(100) and LiF(100), both commensurate and incommensurate phases are seen.[107])

The computed favorable molecular orientations for the isolated CO and CH_3F molecules on NaCl(100)[89] are with molecular axes tilted at roughly 50° to the surface normal. In the case of CO, the calculated electrostatic interactions of the molecular moments with the crystal surface field amount to 2% (dipolar), 38% (quadrupolar), and 37% (octopolar) of the total minimum energy. At monolayer density and low temperature, the experimental spectra indicate[46,108–110] that the CO molecules are oriented perpendicular to the surface with one CO over each Na^+ having the carbon atom down. (Area = 15.8 Å^2 per molecule.) However, at lower temperature, these molecules can tilt away from the surface normal. The infrared spectra for this system can show three vibrational bands, but annealing of the solid eventually produces a spectrum exhibiting a single vibrational band—the other bands are thus associated with edge sites on the small crystallites.

It is interesting to note that the vibrational spectrum for nitrogen adsorbed on NaCl(100)[111] is quite similar to that for CO. Clearly, the intense electric field at this surface induces dipoles in the nitrogen molecules which are infrared active; polarization studies indicate that these dipoles are perpendicular to the surface, and it is reasonable to assume that the molecules are adsorbed directly over the small Na^+ ions where the field is most intense.

Calculations and measurements of the structure and infrared spectra of carbon dioxide on NaCl(100)[46,112–115] indicate that two states dominate at different coverages. For less than $^1/_3$ monolayer, the molecules lie almost flat on the surface and are preferentially over the midpoints between Na^+. As coverage increases (at ~80 K), a condensed film forms with each molecule tilted at an angle of ~37° (calculated) or ~23° (experimental) to the surface plane. The data and the calculations indicate that the structure of the ordered monolayer is commensurate 2 × 1 and contains two CO_2 molecules, which thus corresponds to an area of 15.9 Å^2 per molecule. The calculated energy of the monolayer at 0 K is −29.8 kJ/mol, in reasonable agreement with the experimental value of −30 kJ/mol at 87 K.[110]

The spectrum of acetylene on NaCl(100) has also been measured.[46] The proposed structure for this adsorbed molecule is that it lies at an angle of ~8° to the surface plane in the T-bone lattice with a molecular area that is the same as that for CO_2.

Ab initio calculations of the interaction of CO with the perfect[116] and the stepped[117] LiF(100) surface have been reported. On the perfect surface, the electrostatic part of the interaction is strong enough to stabilize a molecular orientation perpendicular to the surface. The modification of the electrostatic field produced by a step causes a considerable enhancement of the adsorption energy and a reduction in the tilt angle.

The infrared spectra of HBr on LiF(100) has been measured.[118] The polarization data for this system indicate the monolayer HBr is hydrogen bonded to the F^- ions, with the adsorbate molecular axes making angles of $\sim 21°$ to the surface plane.

Recent studies of the structure and spectra of water adsorbed on the NaCl(100) include refs 119–121. The data indicate that a stable monolayer can be grown on this surface at low temperature with a unit cell that is commensurate 2×4 centered rectangular and contains six molecules in a nonplanar hexagonal arrangement (area per molecule = 10.6 Å^2).

There has been considerable interest in adsorption on the (100) face of MgO. Work on this system has been reviewed in ref 122 and recent papers in this area include refs 98 and 123–127. The surface of this solid is highly corrugated because it consists of alternating (large) O^{-2} and (small) Mg^{2+}. There is a large and rapidly changing electric field near the surface as well. Consequently, adsorption energies for simple molecules on this surface would be expected to favor localized adsorption. However, the square symmetry of the (100) plane will produce ordered layers lacking the 6-fold coordination which has the maximum lateral interaction. Instead, a square or at least a centered rectangular crystal would be the preferred structures in localized monolayers on this surface. The diffraction experiments for argon and methane films show layers commensurate with the surface lattice, but with unit cells with edge lengths which are multiples of the MgO surface unit cell length. In particular, a 2×3 commensurate unit cell has been observed for Ar at low temperature, followed by a phase with one-dimensional ordering at $T > 40$ K. For methane, a 2×2 commensurate lattice is found for temperatures up to 80 K. For monolayers of the larger rare gas atoms, incommensurate hexagonal ordering is observed, which illustrates the point that the corrugation seen by a given atom depends very much on the size of the atom relative to the underlying lattice. For ethane on MgO at low temperature, two ordered phases are observed:[127] a $\sqrt{2} \times 2\sqrt{2}$ commensurate phase (area per molecule = 17.7 Å^2) and a phase with an oblique incommensurate unit cell (area = 19.9 Å^2). When these areas are compared with the 21 Å^2 obtained for an ethane molecule lying flat on graphite[128] and 17.1 Å^2 estimated from the bulk crystal parameters, one may conclude that the molecules are lying flat in both phases on MgO(100), with one per unit cell in the oblique and two per unit cell in the commensurate phase.

Monolayers of the quadrupolar gas nitrogen on MgO(100) have also been studied by diffraction and different two-dimensional solids have been identified: three rectangular crystals ($2 \times N$) where the molecules lie in the channels formed by the rows of Mg^{2+} in the surface. Here, N indicates varying adsorbate atom spacing along the channels. At higher temperatures, an ordered hexagonal incommensurate phase is also observed for nitrogen. Experimental values for the orientations of the nitrogen molecules in these monolayers are unknown at present, although it seems likely that tilting occurs in at least some of the phases. Carbon monoxide is quite similar to nitrogen with respect to its physical interactions and thus one might expect the behavior of CO on MgO(100) to be similar to that of N_2. Calculations[123] for these two molecules on MgO indicate that their orientations should be initially flat on the surface. However, the infrared spectra of the CO/MgO system[129–131] are interpreted as being due to CO molecules adsorbed directly over the Mg^{2+} in the intense electric field there, with the carbon atom down. Several vibrational bands are observed, but only one is due to adsorption on the (100) plane of the solid. There appear to be some differences in the translational orderings observed for N_2 and CO, but the orientational behavior in the CO monolayer could well be a model for the N_2.

An important question which arises for MgO is the magnitude of the charges on the ions, since it has been suggested that the binding in this solid is partially covalent and thus, that the ionic charges are significantly less than 2. This question has been explored in connection with the modeling of the NH_3–MgO interactions.[126] Comparison of the calculated energies and experimental indicate that the effective charges for this solid should be close to 2, and that ammonia should adsorb with fixed orientations at low temperature which give rise to large repulsive interactions between neighboring adsorbate molecules and a monolayer capacity which is considerably smaller than that expected for a close-packed layer.

Calculations of the structure and energetics of ammonia and water clusters on MgO(100) have been reported.[132] The conclusion is that water will form a condensed commensurate monolayer on this surface, but ammonia will not. Finally, an *ab initio* calculation of the energetics of Cl_2 on MgO(100) has appeared[133] in which it is argued that the site for Cl_2 adsorption is directly over an oxygen with the adsorbate molecule aligned perpendicular to the surface plane. Energies of adsorption were also calculated and shown to decrease with increasing coverage.

3.4. Adsorption Energy for Gases on Amorphous Solids

Energy contours for a gas atom over an amorphous surface have a very different appearance from those for single crystals. As an example, the energy contours for Kr over a model coal surface are shown in Figure 4. Here, the coal is modeled as an amorphous collection of –CH– groups with Site–Site well depth and size parameters[78] obtained by substituting literature values for the CH–CH and the Kr–Kr interactions into the Lorentz–Berthelot combining rules which are $\epsilon_{XY} = (\epsilon_{XX}\epsilon_{YY})^{1/2}$ and $\sigma_{XY} = (\sigma_{XX} + \sigma_{YY})/2$. Thus, $\epsilon_{Kr\text{-}Site}/k = 101$ K and $\sigma_{Kr\text{-}Site} = 3.45$ Å. Since the coal is modeled as a Bernal solid with a nominally flat surface (coal is actually microporous), direct summation over the Sites gives the interaction energies used to construct the contour diagram. Figure 4 reveals an irregular, heterogeneous surface. The deepest energy wells are blacked in as a guide to the eye—these would ordinarily be described as adsorption sites. However, there is a

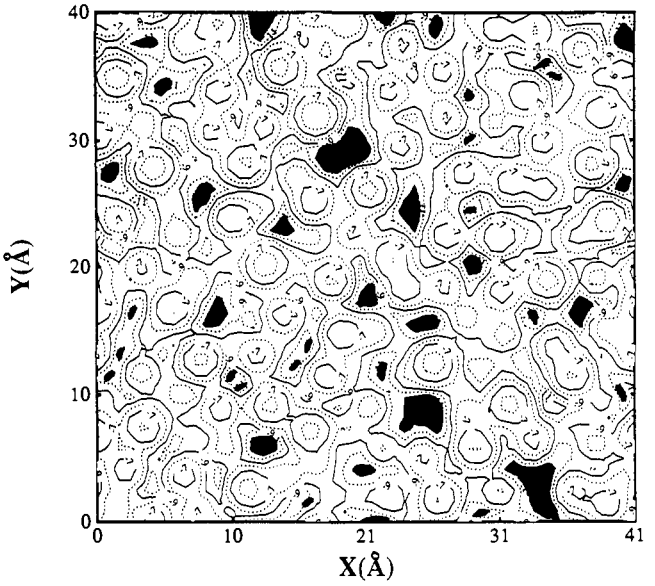

Figure 4. Contours of constant adsorption energy for a krypton atom over an amorphous surface which is designed to model coal. Adsorption energies range from −5.22 to −13.88 kJ/mol, and the contour lines are separated by 1.0 kcal/mol. The regions of strongest adsorption energy have been blacked in as a guide to the eye—they correspond to regions where the energy is less than −11.0 kJ/mol.

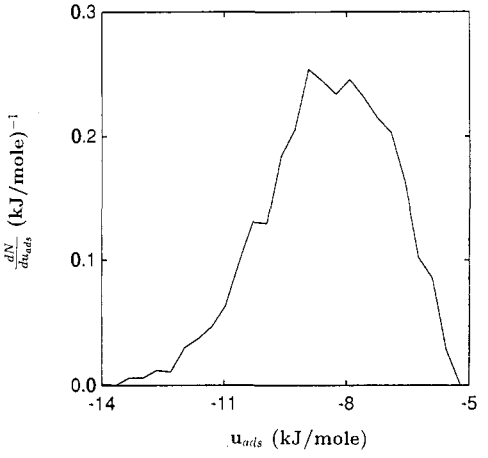

Figure 5. A smoothed histogram of the distribution of adsorption energies for the system shown in Figure 4. The curve is normalized to unit area so that the fraction of the surface with energy in the range between u_{ads} and $u_{ads} + \Delta u_{ads}$ is given by the area of a strip of width Δu_{ads} located at $u_{ads} + 0.5\Delta u_{ads}$.

continuous variation in the Kr–solid energy as the atom moves across the surface and these sites clearly do not correspond to those used in the usual theoretical treatments of adsorption on heterogeneous surfaces which are usually taken to be points on a regular lattice with fixed nearest-neighbor spacings roughly equal to the distance of maximum Kr–Kr interaction. Indeed, the basic descriptor of heterogeneity in these treatments is often taken to be the number distribution of sites with a given adsorption energy.[134,135] It is possible to evaluate a number distribution of adsorption energy from Figure 4 merely by evaluating the histogram of energies for a fine grid of points over the surface. Figure 5 shows such a histogram obtained from a grid of 2500 points (50 × 50 points on a surface which is 40 × 40 Å in size). However, this distribution function is not for the adsorption sites, since the concept of site requires that there be at least a local minimum where the adsorbed atom can attach itself to form a localized species when the temeprature is sufficiently low. The fixed grid will pick up mostly values which are not local minima in τ and will even include local maxima. A better approach would be to identify the local minima and make a histogram of those values only. Even here, there are difficulties since many of the local minima are extremely shallow and will not act as sites at any temperature of interest.

An amorphous surface such as this model of coal will exhibit physical roughness as well as the energetically irregular surface shown in Figure 4. The roughness can be exhibited by a contour plot which is similar to that of Figure 2. One first locates the positions of the minima in the gas–solid energy curves. From these numbers, one can construct the diagram shown in Figure 6. Both parts of this figure are identical contour plots, but the lowest parts of the surface are highlighted in part a, and the highest points, in part b. There is a good correlation between the locations of the strong sites for adsorption shown in Figure 3 and the low spots on the surface shown in Figure 6. The high points are shown because of their possible relevance to diffusion on this surface—it is reasonable to suppose that they may serve as obstacles (or scattering features) for the translational motion of the atoms in the adsorbed monolayer.

One final point is in ordering concerning physical adsorption on heterogeneous surfaces: the weight of the evidence is that complete monolayers on such solids have densities close to two-dimensional close packing, or at least close to what one would expect on the basis of the packing in the bulk liquid near its normal boiling point. This picture is the basis for the use of the BET equation to obtain specific surface area based on monolayer capacity and molecular cross-sectional areas obtained from liquid densities. The success of this approach leads one to the conclusion that heterogeneous surfaces generally will become fully covered with molecules in the monolayer, regardless of the spatial distribution of strong and weak sites. In fact, in one case[75] it has been shown that previously adsorbed molecules help to create new "sites" when a molecule is added to an almost complete monolayer. Although such a molecule interacts weakly with the surface, possibly at a position which was initially a local maximum, favorable interactions with neighboring adsorbate molecules enhance the overall probability of adsorption and thus facilitates completion of the monolayer.

Another class of materials which has been the subject of numerous modeling studies recently is zeolites (see ref 136 and references contained therein). Site–Site models have been heavily exploited in the computer simulation of the thermodynamic, structural, and dynamical properties of gases sorbed in these materials. Since the crystal structure of the aluminosilicate framework is ordinarily known, one uses the positions of the oxides to perform pairwise sums over this part of the lattice, neglecting any Al or Si Site interactions. When cations other than H^+ are also present in the structure, their interactions with the sorbate are included. However, the positions of these species are not always well known, so an element of uncertainty is

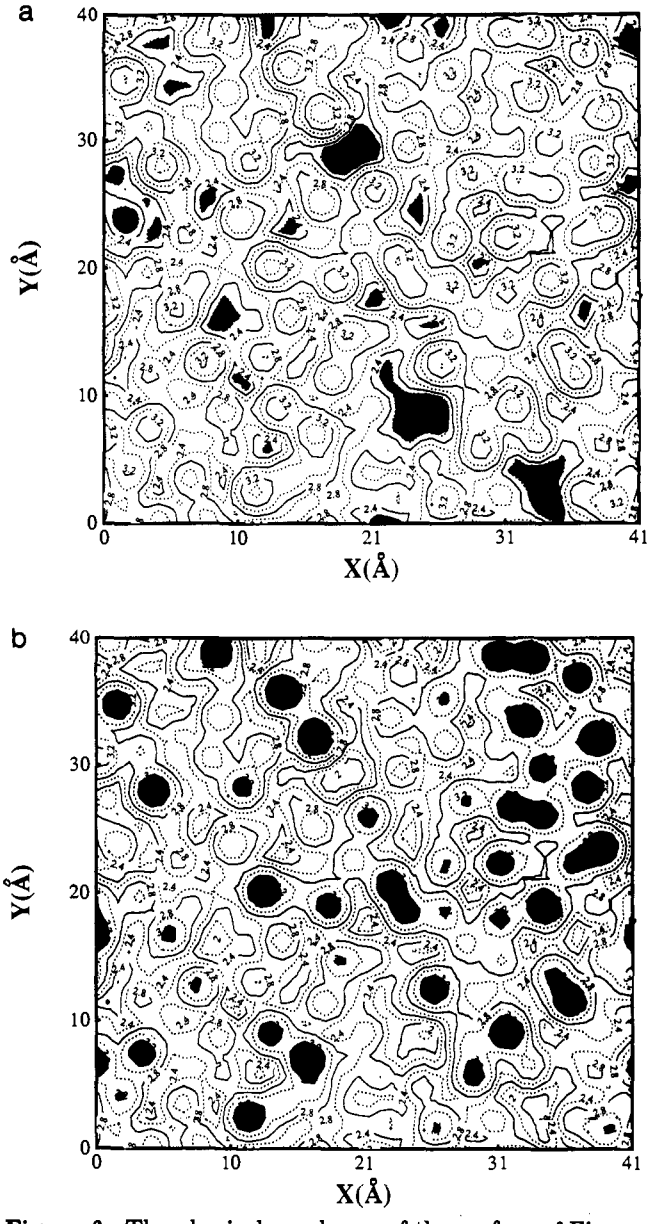

Figure 6. The physical roughness of the surface of Figure 4 is illustrated here by contour lines of constant location of the adsorption energy. The height above the surface of this minimum energy varies by 1.83 Å from the highest to the lowest points. In part a, the lowest regions are blacked in—their locations correspond reasonably well to the locations of the points of strongest adsorption which are shown in Figure 4. In part b, the locations of the highest points over this surface are blacked in.

introduced. Still, comparisons between experimental and simulated data are reasonably good and have led to a number of useful physical insights concerning the locations and nature of adsorption sites and the mobilities of the sorbed species in the complex pore structures of these materials.

Up to this point, the discussion of model potentials has primarily been concerned with atoms interacting with rigid solids. Formally, one can progress to molecules by extending the calculation to allow for more than one interaction Site in the adsorbate molecule. As will be discussed below, molecules such as N_2, O_2, CO, CO_2, and CH_4 are among the many species interacting with the basal plane of graphite which have been modeled in this way. After parametrization of the Site–Site potentials, the results have been used in computer simulations of the structural and thermodynamic properties of the adsorbed films for these materials. One interesting feature of these potentials is that they allow prediction of orientational behavior of the adsorbed molecules relative to the solid surface and each other. Information of this kind is relatively hard to obtain from experiment, especially when one recollects that these orientations are sensitive to both temperature and density.

The representation of molecule–solid potentials presents a problem because now the interaction is a function of six variables, in general (three translational and three orientational). One can still use the Fourier expansion for the τ-dependence of the energy, if τ is taken to be the position of the center-of-mass or center-of-symmetry position of the molecule. However, the orientation-dependence of this energy is often quite significant. One can calculate the potential either as a function of molecule–solid separation distance for various fixed orientations, or one can expand the energy at fixed **r** as a series in suitable angular functions, such as spherical harmonics.[137]

4. Molecular Gases on Graphite

4.1. Potential Functions

Over the years, a considerable effort has been expended in theoretical attempts to evaluate the interaction potentials of rare gases with the graphite basal plane.[5,138–141] However, it appears that the most reliable potentials are still those which have been derived from analysis of the experimental gas–solid virial coefficients as described in section 2. The most questionable aspect of the potentials derived in this way is the magnitude of the corrugation of the interaction, since it appears that the pairwise summation of spherical atom–Site interactions does not yield a sufficiently large periodic variation in the energy. The structures and the thermodynamics of the phases which occur in monolayers adsorbed on the basal plane of graphite are quantities which can be quite sensitive to this energy variation. Complex phase diagrams are observed, with numerous two-dimensional solids as well as two-dimensional liquids and gases found for monatomic and polyatomic adsorbates. Here, we will review the work which is most closely concerned with the intermolecular potentials, both molecule–solid and molecule–molecule. In essence, this means the structure of the two-dimensional solids.

For rare gases, ordered layers which are commensurate with the graphite lattice such as the $\sqrt{3} \times \sqrt{3}$ phase mentioned above for krypton have been observed as well as a variety of solid incommensurate phases. However, the presence of the periodic terms in the gas–solid potential often causes the incommensurate phases to have the unusual property of a variable density which usually takes the form of patches of essentially constant density separated by regions of either higher or lower density which are called domain walls.[142,143] Both incommensurate and commensurate solidlike monolayers have also been found for molecular gases, as will be mentioned below. The extensive studies of the properties of rare gas monolayers on graphite have been reviewed recently[142,144] and will not be discussed further here.

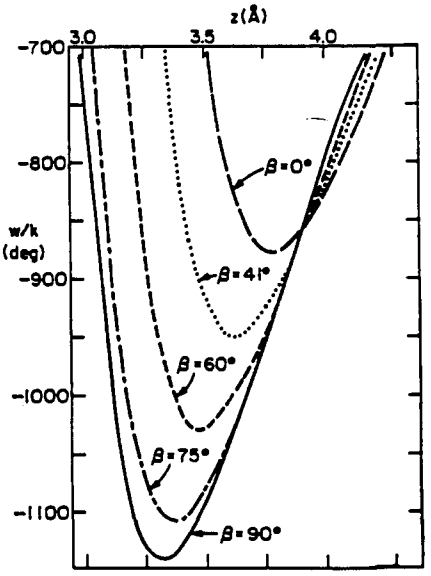

Figure 7. Curves of the surface-averaged interaction of a nitrogen molecule with the graphite basal plane are shown for various values of the orientation angle β between the molecular axis and the surface normal. The energy w/k_B is plotted versus the distance z between the molecular center-of-mass and the surface. (Reprinted from ref 153. Copyright 1977 Editions de Physique.)

Most of the theoretical and simulation studies carried out on molecular monolayers adsorbed on the graphite basal plane have used variants on the simple models for the interaction energy discussed above. That is, the molecule–solid potential is taken to be a pairwise sum over Sites in the molecule which are coincident with the atoms (except for methyl and methylene groups which are frequently approximated as a single Site). Each C atom in the solid is usually taken to be a spherical Site, although there is now reasonably convincing evidence that these carbon Sites are not spherical but more or less ellipsoidal. This idea becomes plausible when one realizes that graphite is quite anisotropic, being more polarizable in directions parallel to the basal plane than perpendicular. Since the attractive part of the dispersion–repulsion interaction is proportional to polarizability in well-known theoretical treatments of the problem, one should take this into account somehow in modeling the Site–Site potentials. When this is done,[145-147] the nonperiodic part of the potential is hardly affected, but the periodic terms become considerably larger than those for spherical C sites. Various estimates for the enhancement range from 50 to 150%, with values at the low end of this range seeming to give the best agreement with experiment.[85,148-152]

When these Site–Site models for the gas–solid interaction are evaluated, one finds large changes in the energy when orientation of the gas molecule relative to the surface is altered. This point is illustrated in Figure 7 which shows calculations of the surface-averaged energy for a nitrogen molecule over the graphite basal plane for different values of the angle between the N_2 molecular axis and the surface normal vector.[153] When the molecule lies parallel to the plane ($\beta = 90°$), a well depth per k_B of −1130 K is found for a molecular center-of-mass distance from the plane equal to 3.3 Å; as the molecule tilts up toward perpendicular, the center-of-mass equilibrium distance moves out to 3.8 Å. At this point, the minimum gas–solid energy per k_B has changed to −880 K, a considerable shift in view of the fact that most experiments on nitrogen adsorption are performed at 100 K or lower.

Table II. Quadrupole Moments for Selected Molecules[a]

molecule	|quadrupole moment| ($C\ m^2 \times 10^{40}$)
nitrogen	4.7
oxygen	1.3
carbon monoxide	8.3
carbon dioxide	13.4
carbon disulfide	12.0
chlorine	11.0
ethane	3.3
ethylene	5.3
acetylene	30.0
benzene	29.0

[a] See refs 154–156.

When considering the lateral interactions for pairs of molecules on the surface, there are good grounds for belief that these potentials are slightly altered relative to the gas-phase curves (see section 5). The main contribution to this change in the effective pair potential is due to the Axilrod–Teller–Muto triple dipole interaction in which one of the three bodies is the solid. For atoms, most of this substrate-mediated effect can be accounted for by decreasing the well-depth parameter by 15–20% relative to the gas-phase value. For molecules, such a reduction has been incorporated into the calculation by using a similar reduction in the Site–Site interaction well depths even though the theoretical justification for this is relatively weak.

The structures and thermodynamic properties of dense adsorbed films are strongly affected by the molecule–molecule interactions as well as the molecule–solid energies. It has emerged that the electrostatic part of the molecule–molecule potentials is particularly important in determining adsorbate molecule orientations in these layers. This is not too surprisng for dipolar adsorbates, but it has been shown that the quadrupolar energies of nonpolar, nonspherical interactions can produce a variety of layer structures, especially for adsorption of the graphite basal plane (see below). Experimental and theoretical quadrupole moments have been reported for many molecules. An abbreviated list is given in Table II. When a pair of quadrupoles is co-planar, as is often the case in monolayers, the electrostatic interaction favors configurations in which the pair forms a T-shape with the two quadrupole moments perpendicular or, with a slightly less favorable value, a parallel arrangement where both moments lie at a 49° angle to the vector connecting them. The most unfavorable arrangements are parallel at angles of either 0° or 90° to the connecting vector. Clearly, this includes pairs of molecules standing perpendicular to the surface. The presence of these interactions significantly affects the orientational arrangements in monolayer (and multilayer) films, especially at low temperature.

The parameters used for molecule Site–C Site potentials are obtained by a combination of techniques. Since Site–Site models have been quite successful in simulations of bulk liquid and solid properties, one can take these potentials as starting points for the molecule–solid problem. Using C Site well depth and size parameters which work well in estimates of the atom–

graphite interaction, one can then try the Lorentz–Berthelot combining rules to obtain a molecule–solid potential. However, in the last analysis the final parameterization of a molecule–graphite potential should be validated by a comparison of calculated and experimental Henry's law constants and/or the zero coverage limiting heat of adsorption. More often than not, this will bring about an adjustment of the well-depth parameters which significantly improves the model interaction.

When the adsorbate molecules of interest possess permanent electrostatic moments, there will be added terms in the molecule–solid energy due, at the least, to the induction of multipoles in the dielectric solid and the interaction between these induced multipoles and the permanent multipoles of the adsorbate molecules. This interaction is usually treated by the method of image charges and is an important aspect of molecules which interact with metal surfaces where the dielectric constant is effectively infinite. However, these interactions are often omitted from molecule–insulator systems. Of course, the fact that one tunes the well-depth parameters by comparison with experiment means that many effects are swept up into the final Site–Site model. Not only the induction energies, but other undoubtedly significant factors like many-body effects (see section 5) will be included in a rough way.

4.2. Monolayer Structures

Perhaps the simplest of the nonspherical molecules are homonuclear diatomics such as O_2 and N_2. Thus, the structures of the monolayers formed by these gases on graphite will be discussed in detail. It emerges that the general features of their behavior also occur in the phases of numerous other simple molecules. For nonpolar, quasilinear molecules, the low-temperature structures of the monolayers are determined by two features of the intermolecular potentials, which are the molecular length-to-breadth ratio and the electrostatic quadrupolar interaction energy. In fact, the structures of many of the observed monolayer crystals can be classified according to their quadrupole moments. For this reason, some relevant values were given in Table II. The data there must be used with caution, since the electrostatic energy of a crystal depends upon molecular separation distance r, with the quadrupolar energy varying as r^{-5}. For example, the calculated quadrupolar energy in the CO_2 monolayer crystal is larger than that in the CS_2 crystal, in spite of the much larger quadrupole moment of CS_2, the similarity of the orientational structures of the two crystals and the dependence of the electrostatic energy upon quadrupole moment squared. However, the CS_2 molecular separations are sufficiently large compared to those for CO_2 to produce this result.

In general, simple nonpolar molecules will lie flat on the surface and be orientationally ordered at very low temperature. However, the ordering is quite different for O_2[157-171] and N_2.[157,167,172-186] Schematic drawings of the molecular arrangements in the low-temperature monolayers for these substances are shown in Figures 8 and 9. The herringbone structure which is found for N_2 is a consequence of the electrostatic quadrupolar interaction between these molecules. In fact, the T-shaped pair and the shifted-parallel pair which are most favorable for quadrupolar interactions are both present in the herringbone array. The Site–Site part of the molecular interaction potentials tends to favor parallel arrangements where the coordination number of a Site is as high as possible (six, or five plus one intramolecular Site, for diatomics in two dimensions), and this is what is found for O_2, which has negligible quadrupolar interactions. The phases of N_2 and O_2 shown in Figures 8 and 9 are the lowest density low-temperature solids, and one can ask whether higher density monolayers are stable, and if they are, what is their structure? It turns out that O_2 exhibits a number of higher density phases which are still characterized by molecules lying flat on the surface and by structures which are incommensurate with the graphite. Their distinctive features are different, fixed orientations of the crystal axes relative to the graphite lattice. This orientational epitaxy was first observed for rare gas

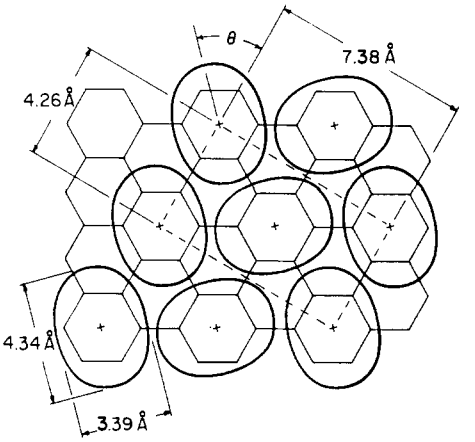

Figure 8. The molecular orientations in the commensurate $\sqrt{3}\times\sqrt{3}$ N_2 monolayer on the graphite basal plane are shown. The ellipses are nitrogen molecules, drawn roughly to scale. The angle θ indicates the orientations in the herringbone pattern; its value is slightly less than 60°. The carbon hexagons in the surface are also shown. In this low-energy commensurate layer, the center of each N_2 lies over the center of a hexagon. (Reprinted from ref 157. Copyright 1983 Asociación Española del Vacio y sus Aplicaciones.)

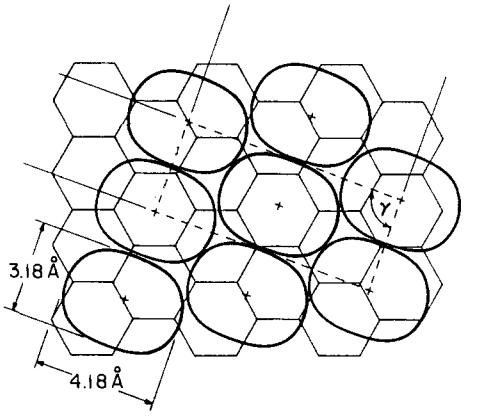

Figure 9. The molecular orientations in the lowest density ordered O_2 monolayer on the graphite basal plane are illustrated. As in Figure 6, the ellipses are adsorbate molecules drawn roughly to scale. The angle γ is very close to 90°, indicating a centered rectangular unit cell. The positions of the centers of these molecules show clearly that this layer is not commensurate with the graphite lattice. (Reprinted from ref 157. Copyright 1983 Asociación Española del Vacio y sus Aplicaciones.)

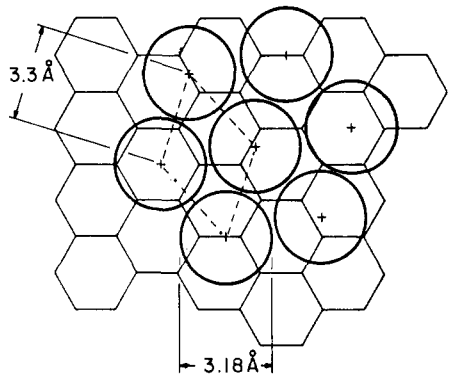

Figure 10. The molecules in the high density O_2 monolayer are shown. Here, the packing is triangular and the circles indicate that the molecules are essentially standing on end in an incommensurate lattice. (From ref 157. Copyright 1983 Asociación Española del Vacio y sus Aplicaciones.)

monolayers and is actually a widespread phenomenon.[187] Its existence is a consequence of the density modulations induced in these two-dimensional crystals by the substrate, as pointed out some time ago.[188] At even higher densities where the molecules in the oxygen monolayer are compressed from the original solid density of 0.073 molecules/Å^2 to a value of 0.11 molecules/Å^2, a phase forms in which the molecules essentially stand on end. The packing of the high density layer is illustrated in Figure 10. (The areas per molecule in these two phases are 13.7 and 9.1 Å^2, respectively.) In contrast, it is rather difficult to increase the density of the N_2 layer from its commensurate value of 0.064 molecules/Å^2 (area per molecule = 15.7 Å^2). Experimentally, one attempts to increase the density in a monolayer by adding more molecules to the system. However, there is always an alternative to the desired density increase, which is adsorption into a second (or higher) layer. When the free-energy change for multilayer formation becomes more favorable than that for additional adsorption into the monolayer, one has in effect reached the upper limit for the monolayer density. In the case of nitrogen, additional adsorption into the commensurate monolayer does occur, with the initial formation of an incommensurate uniaxial phase with a density of ~0.068 molecules/Å^2. Here, the molecules remain in the herringbone pattern and remain flat—some free area between molecules has been squeezed out. At even higher density, another solid has been found where at least some of the molecules are no longer parallel to the surface. There is still some debate about the nature of this phase, with a pinwheel and a 2-out structure having been suggested.[172,176,177,184] In the pinwheel case, a central molecule stands up surrounded by six neighbors which are nearly flat; in the 2-out case, all molecules tilt away from the surface, but are at angles which are not close to perpendicular. The question of which of these two possibilities is most stable is again associated with the electrostatic energy for N_2. Of course, this energy will be large and repulsive for a close-packed array of molecules, all perpendicular to the surface. Both of the two suggested structures give a relatively high areal density without an unfavorable electrostatic energy.

The herringbone ordering found for N_2 is often observed or calculated in the monolayers of other linear molecules on the graphite basal plane, especially when the molecular quadrupole moment provides a significant portion of the adsorbate-adsorbate interaction. Specific cases include the following (all molecules lie flat on the surface except when noted otherwise).

CO_2: Experiment[189] gives an incommensurate, herringbone structure with an area per molecule of 16.1 Å^2 and an angle between nearest-neighbor molecular axes in the herringbone which is equal to ~82°; calculations[186,190] give two structures, depending upon the potential function chosen. Both are incommensurate herringbone, with areas and angles of 16.1 Å^2 and 68° or 17.0 Å^2 and 90°, respectively.

CS_2: Experiment[191] gives an incommensurate rectangular unit cell, herringbone packing, area = 24.3 Å^2 per molecule, angle between molecular axes = 58°. For this system, calculations performed with and without the quadrupolar part of the adsorbate–adsorbate interaction clearly show the change in structure which is produced by this electrostatic energy. When the quadrupole is included, the calculated structure is nearly the same as the experimental herringbone; without it, the molecules are predicted to lie in parallel rows.

C_2N_2: Experiment[192] gives a incommensurate rectangular unit cell, herringbone packing, 24.2 Å^2 per molecule, 70° angle between the axes of nearest neighbor pairs.

CO: Two ordered phases have been observed for CO[179,193,194], a herringbone $\sqrt{3} \times \sqrt{3}$ commensurate and an incommensurate high density pinwheel structure. (The small dipole moment and large quadrupole moment for this molecule make it very similar to N_2. Even the sizes and shapes are very similar.) This is one of the few molecules for which the polarized infrared spectra of the film adsorbed on graphite have been measured.[195] A single vibrational band is found at low temperature which splits as coverage increases. The CO is believed to undergo two-dimensional condensation when this splitting appears. The polarization of the spectra indicate that the transition dipole for this molecule is perpendicular to the surface. Several interpretations of this are possible: the molecules could be oriented perpendicular or they could have a perpendicular dipole induced by an electrostatic field at the surface. (A quadrupolar electric field at the graphite surface has been recently proposed[196] and confirmed experimentally.[197])

C_2H_2: Acetylene[198,199] also forms two monolayers with the molecules lying flat on the surface, a square T where all molecules are perpendicular to one another with a density of 0.053 molecules/Å^2) (area = 18.9 Å^2 per molecule) and a herringbone $\sqrt{3} \times \sqrt{3}$ commensurate phase. In this case, the quadrupole moment is quite large (3.6 times that for CO_2) and the length/width ratio is also comparatively large.

C_2H_4: Ethylene[200-206] shows seven solid monolayer phases. There are two in which the molecular axes lie parallel to the surface. In one, the molecules are orientationally ordered in a centered, almost-rectangular unit cell (with a corner angle = 94° and an area = 19.0 Å^2 per molecule). The second, higher-temperature phase is orientationally disordered and $\sqrt{3} \times \sqrt{3}$ commensurate with two molecules per unit cell (area = 18.3 Å^2 per molecule). This molecule is similar to nitrogen, but the almost-rectangular phase

is incommensurate with the graphite lattice due to the larger area of the ethylene. Furthermore, the fact that the intermolecular distances in the low-temperature crystal are larger for ethylene than for nitrogen means that the quadrupolar energies will be smaller. Presumably, the orientational ordering observed for ethylene is a consequence of the competition between electrostatic and nonelectrostatic contributions to the crystal energy. The five high-density phases have triangular symmetries but different areal densities, presumably reflecting different values of both the tilt angle of the molecular axis and the freedom of rotation around this axis. Three of these phases are commensurate: 2×3 (two per unit cell, area = 17.4 Å^2 per molecule; $\sqrt{3} \times \sqrt{3}$ (also two per unit cell but area = 15.7 Å^2 per molecule); and $2\sqrt{3} \times \sqrt{3}$ (four molecules per unit cell, differing from the previous case only by the orientational ordering one the surface). Finally, an orientationally disordered phase with an area of 15.3 Å^2 per molecule was observed—here, it is likely that the molecules are significantly canted away from the surface plane.

C_2H_6: The ethane monolayer has been studied by several groups.[128,207-213] Here, the molecule is only quasilinear but little is known about its orientation other than that of the C–C bond. Three solids have been observed: a low-density incommensurate herringbone phase with the C–C bonds nearly parallel to the surface, two molecules per unit cell and an area = 19.1 Å^2 per molecule; an intermediate $\sqrt{3} \times 4$ herringbone phase with two molecules per unit cell, an area = 18.2 Å^2 per molecule and a cant angle to the surface of ~16°; and a high-density $\sqrt{3} \times \sqrt{3}$ commensurate phase with the molecules standing more or less on end. An inspection of the quadrupole moments listed in Table II indicates that this molecule can be considered as transitional, with an electrostatic energy which is large enough to produce herringbone structures at relatively low density in the solid, but not large enough to prevent the molecules from standing on end when compressed.

Cl_2: Chlorine[214-216] forms a monolayer qualitatively similar to oxygen. Although the X-ray data indicate a phase in which these molecules are all standing up on the surface with an area = 14.2 Å^2 per molecule, the most recent calculations show also a lower density phase in which the molecules are either in a herringbone or a pinwheel structure depending upon the interaction potential which is used. At this point, it is not clear if either or both interaction potentials are unrealistic. Another possibility is that several ordered phases exist on the graphite surface and further experiments are needed.

Methane is a quasispherical molecule with a size that is well adapted to form a $\sqrt{3} \times \sqrt{3}$ commensurate monolayer on graphite. This system has been extensively studied.[152,217-226] Although the expected commensurate monolayer is observed at low temperature, the system expands slightly into an incommensurate film just before melting. At very low temperature these molecules appearently sit on tripod bases of H atoms.

Structural studies of the monolayers of higher hydrocarbons on graphite are relatively limited,[208,209,227-231] with the exception of benzene. Butane lies flat on the surface and forms an incommensurate rectangular lattice. *n*-Hexane also lies flat, in an ordered herringbone structure which is commensurate in one direction only ($N \times 4\sqrt{3}$) at low density, but becomes $2 \times 4\sqrt{3}$ commensurate at higher density. A number of longer *n*-hydrocarbons have been adsorbed from solution onto graphite and studied by STM. The room temperature monolayer structures of *n*-alkanes containing 27, 32, 34, 36, and 70 carbons have been deduced as well as the structures for several long-chain molecules containing a bulky group or groups along the chain (stearic acid and benzene disubstituted with $C_{12}H_{25}$ are two such). The *n*-alkane molecules lie flat and parallel to one another on the surface with conformations which are all-trans.[232-235] Clearly, all-trans can minimize molecule–solid energies which have been evaluated using the usual Site–Site model.[236] However, a somewhat controversial point arises concerning the orientation of the C–C–C–C planes relative to the surface. One expects that this plane would lie parallel to the surface but the data indicate that commensurate phases form with chain–chain spacings that are roughly 10% too small for minimum energy, if the C–C–C–C planes are parallel to the surface. Rotation of this plane to a perpendicular orientation would give a more favorable chain–chain energy, but a less favorable chain–graphite energy. The balance between these two terms appears to be rather delicate and may well produce a situation where the equilibrium orientation of this plane is temperature and/or solvent dependent. Very recently, X-ray diffraction from these layers[296] has confirmed the STM studies and has extended the measurements to include alkanols adsorbed from solution onto graphite.

Benzene has a reasonably large quadrupole moment which is oriented perpendicular to the molecular plane. Although one would expect this molecule to form a monolayer with all molecules lying flat, this would produce an unfavorable electrostatic interaction. In fact, numerous experimental and computer simulation studies[225,237-243] indicate a single ordered solid that is a commensurate $\sqrt{7} \times \sqrt{7}$ monolayer in which all molecules lie flat on the surface (two molecules per unit cell, area per molecule = 36.6 Å^2). This particular lattice size happens to be very close to recent estimates of the benzene planar van der Waals dimension. In contrast, cyclohexane on graphite[244] forms three ordered phases, including a $\sqrt{7} \times \sqrt{7}$ commensurate phase and two incommensurate phases, one with a hexagonal structure with an edge length ranging from 6.51 to 6.25 Å (compared to 6.51 Å for the commensurate phase) and an even denser phase with a centered rectangular lattice. Toluene on graphite has also been studied[238] and exhibits a 3×3 commensurate phase at low temperature (47.2 Å per molecule) plus an expanded incommensurate phase with a large thermal expansion. It appears that all of these adsorbed molecules lie nearly flat on the surface in their ordered phases.

X-ray diffraction from carbon tetrachloride on graphite shows an incommensurate hexagonal ordered layer with an area of 31.6 Å^2 per molecule.[245,246] Perfluorinated molecules are larger than their hydrocarbon analogues and this fact is reflected in the surface lattices of the molecules of this type which have been studied. SF_6[247] forms a commensurate 2×2 lattice at low temperature (area = 21.0 Å^2 per molecule), but expands into an incommensurate structure at higher temper-

ature. C_2F_6[248] also forms a 2 × 2 lattice at low temperature in which the molecules must be standing on end, and expands to an incommensurate form at higher temperature. CF_4[249] is incommensurate at low temperature (area = 19.4 Å^2 per molecule, depending upon temperature) but expands into the 2 × 2 structure at higher temperature.

Nitric oxide[252] appears to dimerize on the graphite surface to form square N_2O_2 molecules. These form two ordered structures: one with a rectangular unit cell having an area of 25.3 Å^2 per dimer, and one with an oblique cell corresponding to 21.0 Å^2 per dimer.

Structures have been determined for a number of polar molecules on graphite. Since the graphite surface is usually taken to be nonpolar, there are questions concerning the wettability of the surface by strongly polar molecules. From the perspective of adsorption, one has a competition between formation of bulk adsorbate or growth of the adsorbed film whenever more molecules are added to the system. Strong dipolar interactions tend to lower the free energy of the bulk, favoring its formation compared to adsorption on a nonpolar surface where the some of the dipolar interactions are replaced by a rather small molecule–solid energy. When the growth of the adsorbed multilayer film terminates at a finite coverage, it can be said that this is a nonwetting system. One possible consequence is a region of coexistence between adsorbed film and bulk droplets on the solid surface. In the specific case of water on graphite, there is currently a dearth of simulations of this system that employ realistic interaction potentials, and experimental studies of the structural properties of the thin layers on this substrate are also sparse. It does appear that many other polar molecules will form monolayers on graphite, and these monolayers can be highly ordered. Knorr[250] has recently reviewed the structural data for halogenated methanes. The methyl monohalides all lie flat on the surface and form herringbone structures with varying angles of molecular in-plane orientation relative to the unit cell axes. Methyl bromide forms a single uniaxially commensurate monolayer on graphite. However, there are indications that two structures can form at least for methyl fluoride and methyl chloride, with the molecular symmetry axes significantly canted relative to the surface plane. Not surprisingly, the dipole moments of these molecules are generally stacked alternately. Most of the other halogenated methanes form relatively complex structures—for details, see Knorr's article. Potential energy functions for such species are poorly known at present. (However, see ref 251.) It will be interesting to evaluate the effects of the newly determined[197] graphite surface quadrupolar electric field upon the energies and orientations of adsorbed polar molecules.[196]

Finally, experimental monolayer structures for molecules which might be expected to form hydrogen bonds are now beginning to appear. These include methanol,[253] ethanol,[254,255] and imidazole.[256] In all cases, these species essentially lie flat on the surface and form crystals which facilitate zigzig chains of hydrogen bonds. Very recently, the X-ray diffraction from 1-propanol in the monolayer on graphite has been reported.[297] The data indicate the presence of a two-dimensional smectic liquid crystal. Calculations and experiment for ammonia[257,258] indicate that it forms an incommensurate triangular monolayer on graphite in which the dipole moments are somewhat canted relative to parallel to the surface, but otherwise have alternating orientations. (Note that there is still some discrepancy between these results and those obtained earlier in a neutron diffraction study.[217,259])

5. Beyond the Two-Body Site–Site Approximation

Over the years, there have been many attempts to improve upon the semiempirical two-body Site–Site approximation to physical adsorption energies. This work has been reviewed recently,[60,142] so only a brief description of the nature of these calculations and their success will be given here. The research falls into several categories: The first is *a priori* quantum mechanical calculations of the molecule–solid interaction energy. However, this requires accurate calculations of the spatial dependence of the electronic wave functions of both the molecule and the solid. Lack of knowledge of these functions has restricted the number of such calculations and the complexity of the systems considered. Furthermore, the results obtained to date are still inferior to semiempirical interaction curves. A second approach to the problem is to split the energy into attractive and repulsive parts and then treat the two separately. For example, one can treat the attractive part of the potential by adapting the standard theory of dispersion energy to the molecule–solid problem.[260] Although the electronic wave function of any solid is essentially a molecular orbital, it can often be decomposed into sums over atomic orbitals, which then leads one back to the molecule–Site representation. The general theory of the dispersion energy justifies this approach while allowing for different decompositions of the solid wave function into Sites.

At large molecule–solid separation distances, the atomic structures of the two entities are no longer important. This allows one to treat both members of the interacting pair in terms of their macroscopic properties. In particular, one has an exact expression for the coefficient C_3 in the asymptotic dispersion interaction between a polarizable molecule and a dielectric continuum solid. One obtains an energy $-C_3 \times z^{-3}$ with

$$C_3 = \frac{\hbar}{4\pi}\int_{-\infty}^{+\infty} \frac{\epsilon(i\omega) - 1}{\epsilon(i\omega) + 1}\alpha(i\omega)\, d\omega \qquad (14)$$

where $\epsilon(i\omega)$ is the solid dielectric function and $\alpha(i\omega)$ is the adsorbate molecule polarizability, both evaluated at imaginary frequency. Both the dielectric constant and the polarizability can be measured, giving one an accurate calculation of this energy,[261,262] which is closely analogous to the r^{-6} term in the usual expressions for the long range interactions between pairs of molecules. The basic expression can be extended in several ways: The polarizability of the interacting species can be taken to be anisotropic for molecules of symmetry lower than tetrahedral;[263] or, the solid surface can have a nonplanar geometry. Atomic interactions with spherical particles and in cylindrical and spherical pores have been treated in this way.[264,265] It might appear that this asymptotic theory is of little use in adsorption studies since it fails

rather badly at distances near the minimum in the molecule–solid energy. However, it has been shown empirically that there is a good correlation between the actual surface-averaged minimum gas–solid energy and the coefficient C_3 of eq 14.[266] Another less important failing of eq 14 is that it is only the leading term in an infinite series involving polarizabilities of higher order than the dipolar term which is explicitly displayed in eq 14.[267] The first of these arises from the quadrupolar polarizability of the adsorbate molecule and produces an interaction of the form $-C_5z^{-5}$, with the coefficient C_5 given by an expression identical to eq 14 except for the replacement of $\alpha(i\omega)$ by the quadrupole polarizability.[268] A second term which involves quadrupolar induction in the solid has also been treated.[269]

A problem related to the dispersion interaction of a molecule with a dielectric continuum is that of the interaction of a permanent electrostatic moment with a polarizable solid. This is usually treated by the method of images in which the moment induces an image of itself in the dielectric. A contribution to the molecule–solid energy is then generated by the interaction of the electrostatic moment with its image. This can be a significant part of the total for strongly dipolar or quadrupolar adsorbates. In practice, one should somehow take account of the fact that the local dielectric susceptibility determines the magnitude of the image. In addition, this image interaction also depends upon the location of the boundary surface of the dielectric relative to the adsorbate molecule. Since the energies are very sensitive to the location of this boundary,[186] a correct choice is crucial, not only for the case of a permanent moment in the adsorbate, but for the dispersion calculation of eq 14. In fact, the distance dependence of this energy is best written as $C_3/(z-z_s)^3$, where z_s is the location of the boundary of the dielectric solid. Furthermore, introducing atomic structure into a dielectric continuum, especially when the solid is nonconducting (i.e., lacking delocalized electron density) is a difficult problem. Not only does one need to consider the periodic variations in electron density in the solid, but one even has to consider the definition of molecule–solid separation distance when the solid is atomically rough and/or when the decaying electron density which actually defines the termination of the solid extends over a significant distance. For a treatment of this and related problems, see ref 270.

Consider now the repulsive part of the molecule–solid energy in isolation from the attractive terms. Recent treatments of this problem have focused on the local electron density of the substrate as the source for the repulsive interaction.[271,272] Specifically, this energy is taken to be proportional to an integral over the overlapping charge densities of the molecule and the solid, with a proportionality constant which is often taken to be empirical, but rather insensitive to the specific system. To the extent that this approach is quantitatively correct, it has the distinct advantage that all the local effects of atomic structure are naturally included in the results.

Another aspect of this problem which has received some attention recently[273–276] is the role of three-body and higher-order interactions on the attractive part of the molecule–solid potential. The approach taken is to represent the solid as a collection of discrete atoms which interact with a polarizable adsorbate molecule. It is well known that many-body dispersion interactions make a significant contribution to the stabilization energies of solids and liquids, so one should expect similar effects for the molecule–solid energies. These are of two types—for the three-body case, one has Site–Site–atom and Site–atom–atom, where a Site in the adsorbate molecule is here designated by "atom" to distinguish it from a Site in the solid. In the case of the Site–Site–atom energies, which would be given to first order by a sum over the solid of the well-known Axilrod–Teller–Muto terms, the results would tend to be swept up in any semiempirical atom–Site interaction. The only exception to this would be a system where the Site–atom pairwise energies are well known to begin with—for example, a rare gas atom interacting with a solidified rare gas. In this case, the most recent calculations[275,276] do produce a noticeable change of the values obtained from two-body sums. On the other hand, the Site–atom–atom energy, when summed over the solid or when evaluated using a continuum description of the solid, produces a significant change in the adsorbate–adsorbate interaction when both molecules are near or on the surface (see ref 277 and references contained therein). As noted previously, the change reduces the well depth for pairs of atoms or molecules in the monolayer by roughly 15%, an effect that should be included in computer simulation work which is designed to give thermodynamic quantities that will be comparable with experimental data.

6. Physisorption on Metals

6.1. General Theory

The discussion of gases physisorbed on metals has been postponed to this point because gas–metal interactions cannot be realistically represented as a pairwise sum over metallic Sites. The theoretical studies of this problem have recently been reviewed[267] and we will here present only a brief recapitulation of the main ideas, many of which have already been mentioned in the previous section.

The usual procedure is to consider the attractive and repulsive contributions to the interaction separately. In the belief that the attraction is primarily determined by the interaction of the gas atom or molecule with the conduction electrons of the metal, one can begin with eq 14 which gives the energy of interaction of a polarizable atom with a polarizable solid. A series is needed, with the leading term giving the energy due to the gas-induced dipole–solid-induced dipole interaction, followed by terms involving gas-induced quadrupole–solid-induced dipole, the gas-induced dipole–solid-induced quadrupole, and so on. Of course, the presence of a permanent electrostatic moment in the gas molecule will give rise to another series of interactions between the permanent moment (or moments) and the moments induced in the solid. These calculations are reasonably well defined since molecular polarizabilities and multipole moments and metal dielectric susceptibilities are often known quantities, at least for the low-order terms in the series. However, the energies obtained are only accurate in the asymptotic limit of large molecule–solid separation distances, which is not very useful for

calculations of energy near its minimum value. Close to the solid surface, two difficulties are encountered which were mentioned above: the location of the boundary of the dielectric is not easy to determine, and the corrugation of this boundary becomes a concern. In the latter case, one can estimate the corrugation in the energy by assuming that the solid is made up of independent polarizable atoms and performing the pairwise sum, as discussed above.[278] This procedure probably gives an upper limit for the corrugation in the attractive interaction over a metal surface. A third problem in this calculation is associated with the approach of the gas molecule to the surface of the dielectric. This is that overlap between the electrons of the two species affects this generalized dispersion energy by reducing its value. The resulting change in the gas–solid energy is frequently handled by the introduction of an empirical "damping factor" similar to that used in the calculations of gas–gas attractive potentials. The effect of this damping upon the already poorly known corrugation energy is usually ignored.

As noted above, the density functional theory for the repulsive gas–solid energy $E_{rep}(\mathbf{r})$ gives:

$$E_{rep}(\mathbf{r}) = A\rho(\mathbf{r}) \tag{15}$$

where $\mathbf{r}$ is the gas atom position, $\rho(\mathbf{r})$ is the electronic density of the solid, and the constant A depends only weakly upon the nature of the solid. Although this theory seems to work well, one must of course be able to estimate or calculate both $\rho(\mathbf{r})$ and A for the specific gas–metal system under investigation. Attempts to do this are reviewed in ref 267 and, more recently, in ref 279. To the extent the electron density at a metal surface varies with the lateral coordinate τ, a corrugated repulsive potential results.

Rare gas–metal potentials calculated by the techniques described here seem to agree well with available experimental data for a number of single-crystal metal surfaces—some specific cases will be discussed below. Although the theory should be capable of extension to molecules which are explicitly nonspherical, this does not appear to have been seriously studied to date.

Alterations to the interaction potentials of adsorbed atoms or molecules due to the presence of the solid are particularly important in the case of metals.[280] In addition to the usual substrate-mediated effect which is the quantum three-body dispersion interaction discussed above, there is a term in the dispersion interaction part of the gas–solid potential which involves the induction of a dipole in the adsorbate atoms. The magnitudes of these induced dipoles can be estimated from the experimental values of the change in the metal work function upon adsorption and can easily amount to as much as 0.5 D. All these induced dipoles are oriented perpendicular to the surface and thus generate an added repulsive interaction between neighboring adsorbed molecules. This energy varies as $\mu^2 \times d^{-3}$, where d is the separation distance and μ is the induced moment. This dipole moment is related to the work function change $\Delta\Phi$ by $\mu = \Delta\Phi/4\pi n$, where n = number of atoms per unit area. The self-consistent treatment of a two-dimensional array of interacting induced dipoles includes a "depolarization factor" which reduces the effective dipole moment as the coverage increases.

Table III. Selected Well Depths of Surface-Averaged Potentials for Helium on Metal Surfaces

	well depths/k_B (K)	
metal surface	theory[a]	experiment[b]
Ag(100)	83	
Ag(110)	80	70
Ag(111)	85	70–81
Cu(110)	64	73
Au(111)	112	82

[a] See ref 279. [b] See ref 60.

The final result for the energy $E_{\mu\mu}$ due to the placement of these induced dipoles on a triangular lattice can be written as[281]

$$E_{\mu\mu} = (NL\mu^2/2d^3)/(1 + \theta\alpha L/d^3) \tag{16}$$

where N is the number of dipoles, d is now the lattice constant, L is a lattice sum equal to 11.0 for a triangular lattice, θ is the fraction of the lattice sites occupied, and α is the adatom polarizability, which can be up to twice as large as the isolated atom polarizability.

6.2. Gas–Metal Systems

Typical values of the induced dipole moments for isolated rare gas atoms adsorbed on a metal obtained from work function measurements[282] are equal to 0.10, 0.13, and 0.24 D for Ar, Kr, and Xe, respectively, on the Al(111) surface. For xenon on Ag(111), experimental work function changes[283] yield an induced dipole of 0.2 D. From these data plus other information, the various contributions to the lateral interaction energy per mole for a complete monolayer of incommensurate triangularly packed xenon on Ag(111) have been estimated to be as follows:[280] −7430 J, unperturbed Xe–Xe energies; 250 J, vibrational zero-point energy; 150 J, Xe–Xe–Xe triple-dipole dispersion energy; 610 J, substrate-induced dipole energy; and 1200 J, substrate-mediated effects upon the xenon pair interactions. It should be noted that both the substrate-mediated energy and the substrate-induced dipoles are quite sensitive to the value chosen for the xenon–metal separation distance (i.e., the imaging plane). For comparison, the same energies evaluated for Xe on the graphite basal plane are −7470, 260, 150, ~0, and 960.

The numerous experimental studies of molecular beam diffraction from single-crystal metal surfaces have yielded a great deal of quantitative information concerning the interactions of isolated atoms with these surfaces.[102] The selective adsorption resonances yield energy levels for the beam atoms in the surface-averaged potential wells and as noted above, the diffracted intensities yield the surface corrugation. Naturally, the availability of such a large data base has led to extensive theoretical studies of these potentials[267,279] especially for helium. Both the data and the theory are more limited for the isotopes of hydrogen and only a few diffraction studies using neon have been reported. Of the two aspects of the interaction, the surface-averaged potentials appear to be better understood than the corrugations. A limited comparison of theory and experiment for this part of the interaction is given in Table III. The need for an empirical damping function in the calculated attractive interactions is one of several significant sources of uncertainty in the theoretical

Table IV. Selected Well Depths of the Surface-Averaged Potentials for Rare Gases on Metals[a]

gas	Ag(111)	Cu(111)	Cu(110)	Cu(100)	Au(111)
Ne	2.1(1.2*)	1.5	1.4(1.2)	1.5	2.4
Ar	7.8(6.9*)	5.6(8.2*)	5.4	5.5(12.0*)	9.6
Kr	11.6(10.3*)	8.6(14.7,11.5*)	8.2(12.6)	8.4	14.2
Xe	18.3(18.0,21.8,20.3*)	21.7(17.6*)	17.8(19.3*)	19.1(26.0,18.9*)	-(20.6*)

[a] Theoretical values from ref 279; experimental adsorption energies[285] and well depths[60] are shown in parentheses with well depths indicated by asterisk (*). Units are kJ/mol.

numbers. Indeed, several different damping functions have been used.[279,284] In light of this, the level of agreement with experiment is encouraging.

In the case of the heavy rare gases Ar, Kr, and Xe on metals, a range of experimental techniques have been brought to bear. These include diffraction from the ordered rare gas overlayers, electronic spectroscopy, and several types of atomic microscopy as well as the conventional measurements of heats, isotherms, and work functions. As a result, both the gas–metal and the gas–gas interactions of adsorbed atoms can be characterized. The extensive literature on xenon–metal adsorption (and krypton and argon, to a lesser extent) has recently been reviewed[285] in an attempt to show that these systems should be best regarded as chemisorption rather than physisorption. It is now very clear that the perturbation of the xenon atom electronic states is considerable when it is placed on a metal surface. However, the quantitative calculations of interaction potentials are not much affected by the name given to the process.

A selection of the experimental and recent theoretical values for the surface-averaged well depths of the heavier rare gases on single-crystal metal surfaces is given in Table IV. There still remains considerable uncertainty in both types of data for these systems.

One of the interesting features of heavy rare gas adsorption on metals is commensurability of the ordered layers formed at low temperature.[285] We here discuss a single well-known and carefully studied example, which is xenon on Pt(111).[286–289] Several two-dimensional phases form in this system, depending upon temperature and coverage.[290–292] They include a $\sqrt{3} \times \sqrt{3}$ commensurate phase (C) at coverages less than $^1/_3$ the number of Pt atoms in the surface and at temperature between 62 and 99 K. At higher coverage or lower temperature a uniaxially incommensurate phase (IC) forms, followed by a hexagonal incommensurate phase at fractional coverages greater than 0.38. The energy change associated with the C → IC transition amounts to ~2.9 kJ/mol, which is a measure of the energetic corrugation of xenon on this surface. Computer simulations[293] show that the corrugation needed to force the layer from its "natural" atomic spacing of ~4.4 Å to the commensurate spacing of 4.8 Å is considerably larger than initially believed. In a recent paper,[289] it is argued that inclusion of the substrate-mediated effects on the Xe–Xe potential is necessary to obtain approximate agreement with the entire monolayer phase diagram.

In an interesting development, it has been noted that gas–solid interactions on alkali metal surfaces are unusually weak.[60] This effect is particularly striking in the cases of helium and hydrogen on these solids, and both theory and experiment indicate that the wetting behavior of these gases on alkalis is consequently remarkable.[294] In Table V, the attractive energy constants C_3 and the estimated gas-solid well depths are listed for a number of these systems. When one considers that the H_2–H_2 and the He–He pair interaction well depths per k_B are 37 and 10 K, respectively, one begins to suspect that the bulk liquids will be more stable than the dense adsorbed films for some of these systems, and this in fact turns out to be the case for particular ranges of temperature and chemical potential. Measurements of isotherms for He on Cs and H_2 on Rb show the unusual wetting properties which result. Physically, these very small gas–solid energies are a result of rather small C_3 values for the attractive energy (due to the decrease of the dielectric constants of these metals at relatively low frequencies), combined with a repulsive wall which extends unusually far from the outermost plane of metal atoms. This is in turn a consequence of the diffuse electron clouds calculated for alkali metal atoms which, when substituted into eq 15, give $E_{rep}(\mathbf{r})$ that combine with rather small attractive energies to give small well depths at large distances from the surface. This behavior becomes more pronounced as atomic number increases, which leads to the tabulated decrease in well depth as one goes down in the periodic table.

Table V. Gas–Solid Energy Parameters for He and H_2 on Alkali Metals

	Li	Na	K	Rb	Cs
	Hydrogen				
C_3/k_B(K Å^3)	3896	3755	2744	2420	2035
well depth/k_B (K)	88	91	57	44	34
	Helium				
C_3/k_B(K Å^3)	1360	1070	812	754	673
well depth/k_B (K)	17.1	10.4	6.3	5.0	4.4

7. Future Prospects

This review can serve to emphasize the fact that many unsolved problems remain in generating and using potential functions for physisorption. A brief and very personal list will be given here.

Some of these are obvious: for example, a better understanding of adsorption on heterogeneous surfaces remains as a major topic for future work. One needs better modeling for both chemical and geometrical heterogeneity as well as improved statistical mechanical theories to go from the models to the structural and thermodynamic properties. These heterogeneous solids include porous materials, and zeolites in particular. Although the number and variety of such studies is growing, much remains to be done in terms of understanding the behavior of complex species sorbed in porous materials and even with the structures of the sorbates on (or in) these adsorbents under conditions where ordering occurs. It is also clear that much remains

to be done in increasing the accuracy of *ab initio* calculations of gas–solid interaction potentials for all kinds of adsorption systems.

In addition, one expects significant efforts in the near future in several less obvious areas. For instance, the present discussion of physisorption on metals has been limited to rare gas adsorbates, but there is evidence that many molecules can adsorb on these surfaces without dissociating. Relatively unreactive species such as N_2, alkanes, or perfluorinated hydrocarbons are candidates for physisorption on metals, especially at low temperatures where the rate of conversion from physisorption to chemisorption is greatly reduced. Although limited experimental data is now available, theoretical treatments of the interactions of such molecules with metals are lacking.

Another kind of adsorption on metals which is currently a very active area is that of self-assembled monolayers. In this case, the adsorbate molecules are characterized by a reactive group on the end of a hydrocarbon chain. The reactive group chemisorbs on the metal; the hydrocarbon tails interact physically to form a variety of ordered monolayers with different packing densities, tilt angles, and unit cell structures, as determined by STM, AFM, and other structural techniques. Thus, one has combined physi- and chemisorption systems which are excellent candidates for theoretical and simulational studies.

Finally, it is surprising to note the paucity of information concerning the structures and thermodynamics for water adsorbed on well-characterized (preferably, single-crystal) surfaces. Even for such an extensively studied adsorbent as graphite, reliable structural information for water monolayers is remarkably sparse. Furthermore, existing simulation studies of water on nonpolar surfaces are mostly based upon model interactions in which potentially significant features have been omitted. These include periodicity in the gas–solid energies as well as the energies due to the induction of electrostatic multipoles in the solid by the adsorbed water molecules, as well as consideration of the perturbation of the water–water interaction potential by the adsorbent.

Acknowledgments. Financial support from the N.S.F. grant DMR-9022681 is acknowledged. Numerous discussions with Prof. Milton Cole helped greatly in the writing of this review.

References

(1) Steele, W. A. *The Interaction of Gases with Solid Surfaces*; Pergamon Press: Oxford, 1974.
(2) Nicholson, D.; Parsonage, N. G. *Computer Simulation and the Statistical Mechanics of Adsorption* (Academic Press, New York, 1982).
(3) Rowlinson, J. S.; Widom, B. *Molecular Theory of Capillarity*; Oxford University Press: Oxford, 1982; Section 4.2.
(4) Steele, W. A. *J. Phys. Chem.* **1978**, *82*, 817.
(5) Poshkus, D. P. *Disc. Faraday Soc.* **1965**, *40*, 195.
(6) Bojan, M. J.; Steele, W. A. *Langmuir* **1987**, *3*, 116; **1987**, *3*, 1123.
(7) Lajtar, L.; Sokolowski, S. *J. Chem. Soc., Faraday Trans. 1* **1988**, *84*, 19.
(8) Sokolowski, S. *Phys. Lett. A* **1986**, *117*, 468.
(9) Pierotti, R. A. *Chem. Phys. Lett.* **1968**, *2*, 420.
(10) Kiselev, A. V.; Poshkus, D. P. *J. Chem. Soc., Faraday Trans. 2* **1976**, *72*, 950. Kiselev, A. V.; Poshkus, D. P.; Grumadas, A. J. *J. Chem. Soc., Faraday Trans. 1* **1979**, *75*, 1281.
(11) Glandt, E. D. *J. Chem. Phys.* **1981**, *74*, 1321.
(12) Derderian, E. J.; Steele, W. A. *J. Chem. Phys.* **1977**, *66*, 1831.
(13) Jiang, X.-P.; Cole, M. W. *Phys. Rev. B* **1986**, *33*, 2803.
(14) Derderian, E. J.; Steele, W. A. In *Adsorption-Desorption Phenomena*; Ricca, F., Ed.; Academic Press: New York, 1972.
(15) Steele, W. A. *J. Phys. Chem.* **1963**, *67*, 2016.
(16) Jaroniec, M.; Lu, X.; Madey, R. *J. Colloid Interface Sci.* **1991**, *146*, 580.
(17) Cole, M. W.; Holter, N. S.; Pfeifer, P. *Phys. Rev B* **1986**, *33*, 8806.
(18) O'Brien, J. A. *J. Colloid Interface Sci.* **1992**, *149*, 596.
(19) Sokolowski, S.; Stecki, J. *J. Phys. Chem.* **1981**, *85*, 1741.
(20) Stecki, J.; Sokolowski, S. *Mol. Phys.* **1980**, *39*, 343.
(21) Rowlinson, J. S. *Proc. R. Soc. London, A* **1985**, *402*, 67. McQuarrie, D. A.; Rowlinson, J. S. *Mol. Phys.* **1987**, *60*, 977.
(22) Steele, W. A. *Surf. Sci.* **1973**, *39*, 149.
(23) House, W. C.; Jaycock, M. J. *Proc. R. Soc. London, A* **1976**, *348*, 317.
(24) Hoinkes, H. *Rev. Mod. Phys.* **1980**, *52*, 933.
(25) Skofronick, J. G.; Toennies, J. P. In *Surface Properties of Layered Materials*; Benedek, G., Ed.; Kluwer Publishers: Dordrecht, 1992.
(26) *Helium Atom Scattering from Surfaces*; Hulpke, E., Ed.; Springer Series in Surface Sciences; Springer-Verlag: Berlin, 1992; Vol. 27.
(27) Boato, G., Cantini, P.; Guidi, C.; Tantarek, R.; Felcher, G. P. *Phys. Rev. B* **1979**, *20*, 3957.
(28) Chung, S.; Kara, N.; Frankl, D. R. *Surf. Sci.* **1986**, *171*, 45.
(29) Ruiz, J. C.; Scoles, G.; Jonsson, H. *Chem. Phys. Lett.* **1986**, *129*, 139.
(30) Giamello, E.; Pisani, C.; Roetti, C. *Surf. Sci.* **1975**, *49*, 401.
(31) Cole, M. W.; Frankl, D. R.; Goodstein, D. L. *Rev. Mod. Phys.* **1981**, *53*, 199.
(32) Pendry, J. B. *Low Energy Electron Diffraction*; Academic Press: New York, 1974.
(33) White, J. W.; Thomas, R. K.; Trewern, I.; Marlow, I.; Bomchil, G. *Surf. Sci.* **1978**, *76*, 13.
(34) McTague, J. P.; Nielsen, M.; Passell, L. *Crit. Rev. Solid State Sci.* **1979**, *8*, 135.
(35) *Surface X-Ray and Neutron Scattering*; Zabel, J. P., Robinson, I. K. Eds.; Springer Verlag: Berlin, 1991.
(36) Stephens, P. W.; Heiney, P. A.; Birgeneau, R. J.; Horn, P. M.; Moncton, D. E.; Brown, G. S. *Phys. Rev. B* **1984**, *29*, 3512.
(37) Güntherodt, H.-J.; Weisendanger, R. *Scanning Tunneling Microscopy*; Vols. I, II, III, Springer Series in Surface Science, Vols. 20, 28, 29, respectively; Springer Verlag: Berlin, 1992, 1993.
(38) Weiss, P.; Eigler, D. M. *Phys. Rev. Lett.* **1992**, *69*, 2240.
(39) Weiss, P.; Eigler, D. M. In *Manipulation of Atoms at High Fields and Temperatures: Applications*; Votrien, B., Garcia, N., Dransfeld, K., Eds.; Kluwer Publishers: Dordrecht, 1993.
(40) Atamy, F.; Schlögl, R., *Proc. 5th Int. Carbon Conf.*; Essen, June 1992; "Arbeitskreis Kohlenstoff" der Deutschen Keramischen Gesellschaft: Essen, 1992.
(41) Sharp, T. G.; Oden, P. I.; Buseck, P. R. *Surf. Sci.* **1993**, *284*, L405.
(42) Scandella, L.; Kruse, N.; Prins, R. *Surf. Sci.* **1993**, *281*, L331.
(43) Dai, D. J.; Ewing, G. E. *J. Chem. Phys.* **1993**, *98*, 5050.
(44) Quattrocci, L. M.; Ewing, G. E. *J. Chem. Phys.* **1992**, *96*, 4205.
(45) Zehme, S.; Heidberg, J.; Hartmann, H. *Forsch. Kolloid Polym.* **1971**, *55*, 65.
(46) Berg, O.; Quatrocci, L.; Dunn, S. K.; Ewing, G. E. *J. Electron. Spect. Related Phenom.* **1990**, *54/55*, 981.
(47) Cohen De Lara, E.; Kahn, R.; Seloudaix, R. *J. Chem. Phys.* **1985**, *83*, 2646. Kahn, R.; Cohen De Lara, E.; Möller, K. D. *J. Chem. Phys.* **1985**, *83*, 2653.
(48) Heidberg, J.; Meine, D. *Surf. Sci.* **1992**, *279*, L175.
(49) Ramis, G.; Busca, G.; Lorenzelli, V. *Mater. Chem. Phys.* **1991**, *29*, 425.
(50) Meixner, D. L.; Arthur, D. A.; George, S. M. *Surf. Sci.* **1992**, 141.
(51) Evans, J. V.; Whateley, T. L. *Trans. Faraday Soc.* **1967**, *63*, 2769. Fukuda, Y.; Tanabe, K. *Bull. Chem. Soc. Jpn.* **1973**, *46*, 1616. Onishi, H.; Egawa, C.; Aruga, T.; Iwasawa, Y. *Surf. Sci.* **1987**, *191*, 479.
(52) Pacchioni, G. *Surf. Sci.* **1993**, *281*, 207.
(53) Huber, T. E.; Huber, C. A. *Phys. Rev. Lett.* **1987**, *59*, 1120; *Appl. Phys. A* **1990**, *51*, 137.
(54) Beebe, T. P.; Gelin, P.; Yates, J. T., Jr. *Surf. Sci.* **1984**, *148*, 526.
(55) Steele, W. A. *Surf. Sci.* **1973**, *36*, 317.
(56) Hove, J.; Krumhansl, J. A. *Phys. Rev.* **1953**, *92*, 569.
(57) Price, G. L. *Surf. Sci.* **1974**, *46*, 697.
(58) Green, M.; Siewartz, J. *J. Chem. Phys.* **1961**, *35*, 915.
(59) Lennard-Jones, J. E. *Trans. Faraday Soc.* **1928**, *24*, 92; **1932**, *28*, 333.
(60) Vidali, G.; Ihm, G.; Kim, H.-Y.; Cole, M. W. *Surf. Sci. Rep.* **1991**, *12*, 133.
(61) Sokolowski, S. *Phys. Rev. A* **1991**, *44*, 3732.
(62) Heinbuch, U.; Fischer, J. *Phys. Rev. A* **1989**, *40*, 1144.
(63) Schoen, M.; Rhykerd, C. L., Jr.; Cushman, J. H.; Diestler, D. J. *Mol. Phys.* **1989**, *66*, 1171. Schoen, M.; Diestler, D. J.; Cushman, J. H. *J. Chem. Phys.* **1987**, *87*, 5464; **1988**, *88*, 1394; **1991**, *95*, 5432.
(64) MacElroy, J. M. D.; Suh, S.-H. *Mol. Sim.* **1989**, *2*, 313.
(65) Ribarsky, M. W.; Landman, U. *J. Chem. Phys.* **1992**, *97*, 1937.
(66) Somers, S. A.; Davis, H. T. *J. Chem. Phys.* **1992**, *96*, 5389.
(67) Koplik, J.; Banavar, J.; Willemsen, J. F. *Phys. Fluids A* **1989**, *1*, 781.

(68) Trozzi, C.; Ciccotti, G. *Phys. Rev. A* **1984**, *29*, 916.
(69) Thompson, P. A.; Robbins, M. O. *Phys. Rev. Lett.* **1989**, *63*, 766.
(70) Bitsanis, I.; Somers, S. A.; Davis, H. T.; Tirrell, M. *J. Chem. Phys.* **1990**, *93*, 3427.
(71) Mo, G.; Rosenberger, F. *Phys. Rev. A* **1990**, *42*, 4688.
(72) Wandelt, K. In *Chemistry and Physics of Solid Surfaces VIII*; Vanselow, R., Howe, R., Ed.; Springer Series in Surface Science; Springer Verlag: Berlin, 1990; Vol. 22.
(73) Bojan, M. J.; Steele, W. A. *Surf. Sci.* **1988**, *199*, L395; *Langmuir* **1988**, *5*, 625; **1993**, in press.
(74) Finney, J. L. In *Amorphous Metal Alloys*; Luborsky, F. E. Ed.; Butterworths: London, 1983.
(75) Bakaev, V.; Steele, W. A. *Langmuir* **1992**, *8*, 1372; **1992**, *8*, 1379.
(76) Bakaev, V. *Surf. Sci.* **1988**, *198*, 571. Bakaev, V.; Voit, A. V. *Izv. Acad. Nauk SSSR, Ser. Khim.* **1990**, 2007. Bakaev, V.; Chelnokova, O. *Surf. Sci.* **1989**, *296*, 369. Bakaev, V.; Dubinin, M. M. *Dokl. Akad. Nauk SSSR* **1987**, *296*, 369. Bakaev, V. *Izv. Akad. Nauk SSSR, Ser. Khim.* **1988**, 1478.
(77) Bakaev, V.; Steele, W. A. *Langmuir* **1992**, *8*, 148.
(78) Bojan, M. J.; Steele, W. A. *Langmuir* **1992**, *8*, 901.
(79) Brodka, A.; Zerda, T. W. *J. Chem. Phys.* **1991**, *95*, 3710.
(80) Garofalini, S. H. *J. Non-Cryst. Solids* **1990**, *120*, 1. Athanasopoulos, D. C.; Garofalini, S. H. *J. Chem. Phys.* **1992**, *97*, 3775.
(81) MacElroy, J. M. D.; Raghavan, K. *J. Chem. Soc. Faraday Trans.* **1991**, *87*, 1971; *J. Chem. Phys.* **1990**, *93*, 2068. MacElroy, J. M. D. *Langmuir* **1993**, in press.
(82) Kaminsky, R. D.; Monson, P. A. *J. Chem. Phys.* **1991**, *95*, 2936.
(83) Demi, T.; Nicholson, D. *Langmuir* **1991**, *7*, 2342. Demi, T. *J. Chem. Phys.* **1991**, *95*, 9242. Demi, T.; Nicholson, D. *Mol. Sim.* **1991**, *5*, 363; **1991**, *7*, 121.
(84) Pisani, C.; Ricca, F.; Roetti, C. *J. Phys. Chem.* **1973**, *77*, 657.
(85) Suh, S.-H.; Lermer, N.; O'Shea, S. F. *Chem. Phys.* **1989**, *129*, 273.
(86) *The Fractal Approach to Heterogeneous Chemistry*; Avnir, D., Ed.; John Wiley: New York, 1989.
(87) Pfeifer, P. *Springer Ser. Surf. Sci.* **1988**, *10*, 283. Pfeifer, P.; Cole, M. W. *New J. Chem.* **1990**, *14*, 221.
(88) Ricca, F.; Pisani, C.; Garrone, E. *J. Chem. Phys.* **1969**, *51*, 4099. Ricca, F.; Garrone, E. *Trans. Faraday Soc.* **1970**, *66*, 959.
(89) Lakhlifi, A. *Mol. Phys.* **1993**, *78*, 659.
(90) Herzfeld, K. F. *J. Am. Chem. Soc.* **1929**, *51*, 2608.
(91) Orr, W. J. C. *Trans Faraday Soc.* **1939**, *35*, 1247.
(92) Lenel, F. V. *Z. Phys. Chem. B* **1933**, *33*, 379.
(93) Hayakawa, T. *Bull. Chem. Soc. Jpn.* **1957**, *30*, 124; 236; 243; 332; 337.
(94) Marcovitch, O.; Kozirovski, Y. *J. Chem. Soc. Faraday Trans. 2* **1975**, *71*, 1302.
(95) House, W. A.; Jaycock, M. J. *J. Colloid Interface Sci.* **1977**, *59*, 266.
(96) Ben Ephraim, A.; Folman, M. *J. Chem. Soc., Faraday Trans. 2* **1976**, *72*, 671.
(97) House, W. A.; Jaycock, M. J. *J. Chem. Soc. Faraday Trans. 2* **1974**, *70*, 1348.
(98) Guo, Z.-C.; Bruch, L. W. *J. Chem. Phys.* **1992**, *97*, 7748.
(99) Gready, J. E.; Bacskay, G. B.; Hush, N. S. *Chem. Phys.* **1978**, *31*, 1978.
(100) Polanyi, J. C.; Williams, R. J.; O'Shea, S. F. *J. Chem. Phys.* **1991**, *94*, 978.
(101) Huang, Z.-H.; Guo, H. *J. Chem. Phys.* **1993**, *98*, 7412.
(102) Hoinkes, H.; Wilsch, H. In *Helium Atom Scattering from Surfaces*; Hulpke, E., Ed.; Springer-Verlag: Berlin, 1992.
(103) Fowler, P. W.; Hutson, J. M. *Phys. Rev. B* **1986**, *33*, 3724. Hutson, J. M.; Fowler, P. W. *Surf. Sci.* **1986**, *173*, 337.
(104) Eichenauer, D.; Toennies, J. P. *Surf. Sci.* **1988**, *197*, 337.
(105) Tatewaki, H.; Nakamura, T. *Surf. Sci.* **1981**, *108*, L447.
(106) Glachant, A.; Coulomb, J.; Biberian, J. P. *Surf. Sci.* **1976**, *59*, 619. Glachant, A.; Bardi, U. *Surf. Sci.* **1979**, *87*, 187. Bardi, U.; Glachant, A.; Bienfait, M. *Surf. Sci.* **1980**, *97*, 137.
(107) Robinson, G. N.; Camillone, N., III; Rowntree, P. A.; Liu, G.-Y.; Wang, J.; Scoles, G. *J. Chem. Phys.* **1992**, *96*, 9212.
(108) Richardson, H. H.; Baumann, C.; Ewing, G. E. *Surf. Sci.* **1987**, *185*, 15. Chang, H.-C.; Richardson, H. H.; Ewing, G. E. *J. Chem. Phys.* **1988**, *89*, 7561. Noda, C.; Ewing, G. E. *Surf. Sci.* **1990**, *240*, 181. Disselkamp, R.; Chang, H.-C.; Ewing, G. E. *Surf. Sci.* **1990**, *240*, 193.
(109) Heidberg, J.; Stahmer, K.; Stein, H.; Weiss, H.; Folman, M. *Z. Phys. Chem.* **1987**, *155*, 223. Heidberg, J.; Kampshoff, E.; Kühnemuth, R.; Suhren, M.; Weiss, H. *Surf. Sci.* **1992**, *269/270*, 128.
(110) Heidberg, J.; Kampshoff, E.; Kühnemuth, R.; Schönekäs, O.; Suhren, M. *J. Electron. Spect. Related Phenom.* **1990**, *54/55*, 945.
(111) Richardson, H. H.; McDonald, T. L.; *J. Electron. Spect. Related Phenom.* **1990**, *54/55*, 1003.
(112) Berg, O.; Ewing, G. E. *Surf. Sci.* **1989**, *220*, 207. Berg, O.; Disselkamp, R.; Ewing, G. *Surf. Sci.* **1992**, *277*, 8.
(113) Heidberg, J.; Kampshoff, O.; Schönekäs, O.; Stein, H.; Weiss, H. *Ber. Bunsen-Ges. Phys. Chem.* **1990**, *94*, 112; 118; 127. Heidberg, J.; Kampshoff, E.; Kühnemuth, R.; Schönekäs, O. *Surf. Sci.* **1992**, *272*, 306; **1992**, *269/270*, 120.
(114) Lange, G.; Toennies, J. P.; Vollmer, R.; Weiss, H. *J. Chem. Phys.* **1993**, *98*, 10096.
(115) Schimmelpfennig, J.; Fölsch, S.; Henzler, M. *Verh. Deutsch Phys. Ges.* **1990**, *4*, 192.
(116) Causà, M.; Dovesi, R.; Ricca, F. *Surf. Sci.* **1993**, *280*, 1.
(117) Pisani, C.; Corà, F.; Orlando, R.; Nada, R. *Surf. Sci.* **1993**, *282*, 185.
(118) Blass, P. M.; Jackson, R. C.; Polanyi, J. C.; Weiss, H. *J. Electron Spect. Related Phenom.* **1990**, *54/55*, 993.
(119) Heidberg, J.; Häser, W. *J. Electron Spect. Related Phenom.* **1990**, *54/55*, 971.
(120) Fölsch, S.; Stock, A.; Henzler, M. *Surf. Sci.* **1992**, *264*, 65.
(121) Wasserman, B.; Mirbt, S.; Reif, J.; Zink, J C.; Matthias, E. *J. Chem. Phys.* **1993**, *98*, 10049.
(122) Coulomb, J. P. In *Phase Transitions in Surface Films 2*; Taub, H., Torzo, G., Lauter, H. J., Fain, S. C., Jr., Eds.; NATO ASI 267; Plenum Press: New York, 1991.
(123) Lakhlifi, A.; Girardet, C. *Surf. Sci.* **1991**, *241*, 400.
(124) Dovesi, R.; Orlando, R.; Ricca, F.; Roetti, C. *Surf. Sci.* **1987**, *186*, 267 and references therein.
(125) Alavi, A.; McDonald, I. *Mol. Phys.* **1990**, *69*, 703. Alavi, A. *Mol. Phys.* **1990**, *71*, 1173. Alavi, A. *Phys. Rev. Lett.* **1990**, *64*, 2289.
(126) Picaud, S.; Lakhlifi, A.; Girardet, C. *J. Chem. Phys.* **1993**, *98*, 3488.
(127) Sidoumou, M.; Angot, T.; Suzanne, J. *Surf. Sci.* **1992**, *272*, 347.
(128) Gay, J.-M.; Suzanne, J.; Wang, R. *J. Chem. Soc. Faraday Trans. 2* **1986**, *82*, 1669.
(129) Scarano, D.; Spoto, G.; Bordiga, S.; Coluccia, S.; Zecchina, A. *J. Chem. Soc. Faraday Trans.* **1992**, *88*, 291. Platero, E. E.; Scarano, D.; Spoto, G.; Zecchina, A. *Faraday Disc. Chem. Soc.* **1985**, *80*, 183.
(130) He, J.-W.; Estrada, C. A.; Corneille, J. S.; Wu, M.-C.; Goodman, D. W. *Surf. Sci.* **1992**, *261*, 164.
(131) Marchese, L.; Coluccia, S.; Martra, G.; Zecchina, A. *Surf. Sci.* **1992**, *269/270*, 135.
(132) Picaud, S.; Hoang, P. N. M.; Girardet, C. *Surf. Sci.* **1992**, *278*, 339.
(133) McCarthy, M. I.; Hess, A. C. *J. Chem. Phys.* **1992**, *96*, 6010; **1993**, *98*, 6387.
(134) Jaroniec, M.; Madey, R. *Physical Adsorption on Heterogeneous Surfaces*; Academic Press: New York, 1988.
(135) Rudzinski, W.; Everett, D. *Adsorption of Gases on Heterogeneous Surfaces*; Academic Press: New York, 1992.
(136) Vernov, A. V.; Steele, W. A.; Abrams, L. *J. Phys. Chem.* **1993**, *97*, 7660.
(137) van den Berg, T. H. M.; van der Avoird, A. *Phys. Rev. B* **1989**, *40*, 1932.
(138) Freeman, D. L. *J. Chem. Phys.* **1975**, *62*, 941.
(139) Toigo, F.; Cole, M. W. *Phys. Rev. B* **1985**, *32*, 6989.
(140) Sharma, S. R.; O'Shea, S. F.; Meath, W. J. *Phys. Rev. B* **1989**, *40*, 6356.
(141) Vidali, G.; Cole, M. W.; Schwartz, C. *Surf. Sci.* **1979**, *87*, L273.
(142) Shrimpton, N. D.; Cole, M. W.; Steele, W. A.; Chan, M. W. C. In *Surface Properties of Layered Materials*; Benedek, G., Ed.; Kluwer Publishers: Dordrecht, 1992.
(143) Kern, K.; Comsa, G. In *Phase Transitions in Surface Films 2*; Taub, H., Torzo, G., Lauter, H. J., Fain, S. C., Jr., Eds.; NATO ASI 267; Plenum Press: New York, 1991.
(144) Chan, M. H. W. In *Phase Transitions in Surface Films 2*; Taub, H., Torzo, G., Lauter, H. J., Fain, S. C., Jr., Eds.; NATO ASI 267; Plenum Press: New York, 1991.
(145) Carlos, W. E.; Cole, M. W. *Surf. Sci.* **1980**, *91*, 339. Vidali, G.; Cole, M. W. *Phys. Rev. B* **1984**, *29*, 6736.
(146) Crowell, A. D. *Surf. Sci.* **1981**, *111*, L667. Brown, J. S.; Crowell, A. D. *Surf. Sci.* **1984**, *146*, 61. Crowell, A. D.; Brown, J. S. *Surf. Sci.* **1982**, *123*, 296.
(147) Bonino, G.; Pisani, C.; Ricca, F.; Roetti, C. *Surf. Sci.* **1975**, *50*, 379.
(148) Bruch, L. W. In *Phase Transitions in Surface Films 2*; Taub, H., Torzo, G., Torzo, G., Lauter, H. J., Fain, S. C., Jr., Eds.; NATO ASI 267; Plenum Press: New York, 1991.
(149) Shrimpton, N. D.; Steele, W. A. *Phys. Rev. B* **1991**, *44*, 3297.
(150) Hansen, F. H.; Frank, V. L. P.; Taub, H.; Bruch, L. W.; Lauter, H. J.; Dennison, J. R. *Phys. Rev. Lett.* **1990**, *64*, 764.
(151) Bhethanabotla, V.; Steele, W. A. *J. Phys. Chem.* **1988**, *92*, 3285.
(152) Kim, H.-Y.; Steele, W. A. *Phys. Rev. B* **1992**, *45*, 6226.
(153) Steele, W. A. *J. Phys. (Paris)* **1977**, *38*, C4–61.
(154) Graham, C.; Pierrus, J.; Raab, R. E. *Mol. Phys.* **1989**, *67*, 939.
(155) Amos, R. D.; Battaglia, M. R. *Mol. Phys.* **1978**, *36*, 1517. Amos, R. D.; Williams, J. H. *Chem. Phys. Lett.* **1979**, *66*, 471.
(156) Buckingham, A. A.; Disch, R. L.; Dunmur, D. A. *J. Am. Chem. Soc.* **1968**, *90*, 3104. Buckingham, A. D.; Graham, C.; Williams, J. H. *Mol. Phys.* **1983**, *49*, 703. Battaglia, M. R.; Buckingham, A. D.; Williams, J. H. *Chem. Phys. Lett.* **1981**, *78*, 421. Battaglia, M. R.; Buckingham, A. D.; Neumark, D.; Pierens, R. K.; Williams, J. H. *Mol. Phys.* **1981**, *43*, 1015.
(157) Diehl, R. D.; Fain, S. C., Jr. *Phys. Rev. B* **1982**, *26*, 4785. Fain, S. C., Jr.; Toney, M. F.; Diehl, R. D. In *Proceedings of the Ninth International Vacuum Congress and Fifth International Conference on Solid Surfaces*; de Segovia, J. L., Ed.; Imprenta Moderna: Madrid, 1983; p 129.
(158) Flurchick, K.; Etters, R. D. *J. Chem. Phys.* **1986**, *84*, 4657.
(159) Morishige, K.; Mimata, K.; Kittaka, S. *Surf. Sci.* **1987**, *192*, 197.
(160) Krim, J.; Coulomb, J. P.; Bouzidi, J. *Phys. Rev. Lett.* **1987**, *58*, 583.
(161) Etters, R. D.; Pan, R.-P.; Chandrasekharan, V. *Phys. Rev. Lett.* **1980**, *45*, 645. Pan, R.-P.; Etters, R. D.; Kobashi, K.; Chandrasekharan, V. *J. Chem. Phys.* **1982**, *77*, 1035.
(162) Mochrie, S. J. G.; Sutton, M.; Akimitsu, J.; Birgeneau, R. J.; Horn, P. M.; Dimon, P.; Moncton, D. E. *Surf. Sci.* **1984**, *138*, 599.

(163) Joshi, Y. P.; Tildesley, D. J. *Surf. Sci.* **1986**, *166*, 169.
(164) Toney, M. F.; Diehl, R.; Fain, S. C., Jr. *Phys. Rev. B* **1983**, *27*, 6413.
(165) Bhethanabotla, V.; Steele, W. A. *Langmuir* **1987**, *3*, 581.
(166) Heiney, P. A.; Stephens, P. W.; Mochrie, S. G. J.; Akimitsu, J.; Birgeneau, R. J.; Horn, P. M. *Surf. Sci.* **1983**, *125*, 539.
(167) Nielsen, M.; Ellenson, W. D.; McTague, J. P. In *Neutron Inelastic Scattering*; International Atomic Energy Agency: Vienna, 1978; Vol. 1.
(168) Nielsen, M.; McTague, J. P. *Phys. Rev. B* **1979**, *19*, 3096.
(169) Bhethanabotla, V.; Steele, W. A. *Phys. Rev. B* **1990**, *41*, 9480.
(170) Toney, M. F.; Fain, S. C., Jr. *Phys. Rev. B* **1987**, *36*, 1248.
(171) Guest, R. J.; Nilsson, A.; Björneholm, O.; Hernnäs, B.; Sandell, A.; Palmer, R. E.; Mårtensson, N. *Surf. Sci.* **1992**, *269/270*, 432.
(172) Wang, R.; Wang, S.-K.; Taub, H.; Newton, J. C.; Shechter, H. *Phys. Rev. B* **1987**, *35*, 5841. Wang, S.-K.; Newton, J. C.; Wang, R.; Taub, H.; Dennison, J. R.; Shechter, H. *Phys. Rev. B* **1989**, *39*, 10331.
(173) Kjems, J. K.; Passell, L.; Taub, H.; Dash, J. G.; Novaco, A. D. *Phys. Rev. B* **1976**, *13*, 1446.
(174) Eckert, J.; Ellenson, W. D.; Hastings, J. B.; Passell, L. *Phys. Rev. Lett.* **1979**, *43*, 1329.
(175) Diehl, R. D.; Toney, M. F.; Fain, S. C., Jr. *Phys. Rev. Lett.* **1982**, *48*, 177. Diehl, R. D.; Shaw, C. D.; Fain, S. C., Jr.; Toney, M. F. In *Ordering in Two Dimensions*; Sinha, S., Ed.; Elsevier-North Holland: New York, 1980.
(176) You, H.; Fain, S. C., Jr. *Faraday Disc. Chem. Soc.* **1985**, *80*, 159.
(177) Peters, C.; Klein, M. *Phys. Rev. B* **1985**, *32*, 6077.
(178) Mouritsen, O. G.; Berlinsky, A. J. *Phys. Rev. Lett.* **1982**, *48*, 181.
(179) Morishige, K.; Mowforth, C.; Thomas, R. K. *Surf. Sci.* **1985**, *151*, 289.
(180) Talbot, J.; Tildesley, D. J.; Steele, W. A. *Surf. Sci.* **1986**, *169*, 71. Talbot, J.; Tildesley, D. J.; Steele, W. A. *Mol. Phys.* **1984**, *51*, 1331. Lynden-Bell, R. M.; Talbot, J.; Tildesley, D. J.; Steele, W. A. **1985**, *54*, 183.
(181) Migone, A. D.; Kim, H.-K.; Chan, M. H. W.; Talbot, J.; Tildesley, D. J.; Steele, W. A. *Phys. Rev. Lett.* **1983**, *51*, 192.
(182) Steele, W. A.; Vernov, A. *Surf. Sci.* **1986**, *171*, 83.
(183) Fain, S. C., Jr. *Ber. Bunsen-Ges. Phys. Chem.* **1986**, *90*, 211.
(184) Bhethanabotla, V.; Steele, W. A. *J. Chem. Phys.* **1989**, *91*, 4346.
(185) Kuchta, B.; Etters, R. D. *Phys. Rev. B* **1987**, *36*, 3407.
(186) Bruch, L. W. *J. Chem. Phys.* **1983**, *79*, 3148.
(187) Grey, F.; Bohr, J. In *Phase Transitions in Surface Films 2*; Taub, H., Torzo, G., Lauter, H. J., Fain, S. C., Jr., Eds.; NATO ASI 267; Plenum Press: New York, 1991.
(188) Novaco, A. D. *Phys. Rev. B* **1979**, *19*, 6493. Novaco, A. D.; McTague, J. P. *Phys. Rev. Lett.* **1977**, *38*, 1286; *J. Phys. (Paris)* **1977**, *38*, C4–116.
(189) Morishige, K. *Mol. Phys.* **1993**, *78*, 1203.
(190) Hammonds, K. D.; McDonald, I. R.; Tildesley, D. J. *Mol. Phys.* **1990**, *70*, 175.
(191) Joshi, Y. P.; Tildesley, D. J.; Ayres, J. S.; Thomas, R. K. *Mol. Phys.* **1988**, *65*, 991.
(192) Terlain, A.; Larher, Y.; Angerand, F.; Parette, G.; Lauter, H.; Bassignana. *Mol. Phys.* **1986**, *58*, 799.
(193) Belak, J.; Kobashi, K.; Etters, R. D. *Surf. Sci.* **1985**, *161*, 390.
(194) You, H.; Fain, S. C., Jr. *Surf. Sci.* **1985**, *151*, 361. Fain, S. C., Jr.; You, H. In *Proceedings of the First International Conference on the Structure of Surfaces*, Berkeley, CA, 1984; Springer Verlag: Berlin, 1985.
(195) Heidberg, J.; Warskular, M. *J. Electron. Spect. Related Phenom.* **1990**, *54/55*, 961.
(196) Vernov, A. V.; Steele, W. A. *Langmuir* **1991**, *8*, 155.
(197) Whitehouse, D. B.; Buckingham, A. D. *J. Chem. Soc., Faraday Trans.* **1993**, *89*, 1909.
(198) Thorel, P.; Marti, C.; Bomchil, G.; Alloneau, J. M. *Suppl. Le Vide, Les Couches Minces* **1980**, *1*, 119.
(199) Peters, C.; Morrison, J. A.; Klein, M. L. *Surf. Sci.* **1986**, *165*, 355.
(200) Larese, J. Z.; Passell, L.; Ravel, B. *Can. J. Chem.* **1988**, *66*, 633.
(201) Moller, M.; Klein, M. L. *Chem. Phys.* **1989**, *129*, 235.
(202) Seguin, J. L.; Suzanne, J. *Surf. Sci. Lett.* **1982**, *118*, L241.
(203) Sutton, M.; Mochrie, S. G. J.; Birgeneau, R. J. *Phys. Rev. Lett.* **1983**, *51*, 407.
(204) Nosé, S.; Klein, M. *Phys. Rev. Lett.* **1984**, *53*, 818.
(205) Satija, S. K.; Passell, L.; Eckert, J.; Ellenson, W.; Patterson, H. *Phys. Rev. Lett.* **1983**, *51*, 411.
(206) Eden, V. L.; Fain, S. C., Jr. *Phys. Rev. B* **1991**, *43*, 10697; *J. Vac. Sci. Tech. A* **1992**, *10*, 2227.
(207) Gay, J.-M.; Suzanne, J.; Wang, R. *J. Phys. Lett. (Paris)* **1985**, *46*, 425.
(208) Hansen, F. Y.; Taub, H. *Phys. Rev. B* **1979**, *19*, 6542. Hansen, F. Y.; Taub, H. In *Phase Transitions in Surface Films 2*; Taub, H., Torzo, G., Lauter, H. J., Fain, S. C., Jr., Eds.; NATO ASI 267; Plenum Press: New York, 1991.
(209) Taub, H.; Trott, G. J.; Hansen, F. Y.; Danner, H. R.; Coulomb, J. P.; Biberian, J. P.; Suzanne, J.; Thomy, A. In *Ordering in Two Dimensions*; Sinha, S., Ed.; Elsevier-North Holland: New York, 1980.
(210) Osen, J. W.; Fain, S. C., Jr. *Phys. Rev. B* **1987**, *36*, 4074.
(211) Suzanne, J.; Seguin, J. L.; Taub, H.; Biberian, J. P. *Surf. Sci.* **1983**, *125*, 153.
(212) Moller, M.; Klein, M. L. *J. Chem. Phys.* **1989**, *90*, 1960.
(213) Hansen, F. Y.; Taub, H. *J. Chem. Phys.* **1983**, *87*, 3232. Hansen, F. Y.; Alldredge, G. P.; Bruch, L. W.; Taub, H. *J. Chem. Phys.* **1985**, *83*, 348. Hansen, F. Y.; Taub, H. *Phys. Rev. B* **1979**, *19*, 6542.
(214) Klee, H.; Knorr, K.; Weichert, H. *Surf. Sci.* **1986**, *171*, 103.
(215) Hammonds, K. D.; McDonald, I. R.; Tildesley, D. J. *Mol. Phys.* **1993**, *78*, 173.
(216) Suh, S.-H.; O'Shea, S. F. *Can. J. Chem.* **1988**, *66*, 955.
(217) Marlow, I.; Thomas, R. K.; Trewern, T. D. *J. Phys. (Paris)* **1977**, *38*, C4–19.
(218) Severin, E. S.; Tildesley, D. J. *Mol. Phys.* **1980**, *41*, 1401.
(219) Glachant, G.; Coulomb, J. P.; Bienfait, M.; Thorel, P.; Marti, C.; Dash, J. G. In *Ordering in Two Dimensions*; Sinha, S., Ed.; Elsevier-North Holland: New York, 1980.
(220) Dutta, P.; Sinha, S. K.; Vora, P.; Neilsen, M.; Passell, L.; Bretz, M. In *Ordering in Two Dimensions*; Sinha, S., Ed.; Elsevier-North Holland: New York, 1980.
(221) Beaume, R.; Suzanne, J.; Coulomb, J. P.; Glachant, A.; Bomchil, G. *Surf. Sci.* **1984**, *137*, L117.
(222) Gay, J. M.; Dutheil, A.; Krim, J.; Suzanne, J. *Surf. Sci.* **1986**, *177*, 25.
(223) Phillips, J. M. *Phys. Rev. B* **1984**, *29*, 4821, 5865. Phillips, J. M.; Hammerbacher, M. D. *Phys. Rev. B* **1984**, *29*, 5859.
(224) Vora, P.; Sinha, S.; Crawford, R. K. *Phys. Rev. Lett.* **1979**, *43*, 704.
(225) Battezzati, L.; Pisani, C.; Ricca, F. *J. Chem. Soc., Faraday Trans. 2* **1975**, *71*, 1629.
(226) Glachant, A.; Coulomb, J. P.; Bienfait, M.; Dash, J. G. *J. Phys. Lett. (Paris)* **1979**, *40*, L543.
(227) Hansen, F. Y.; Newton, J. C.; Taub, H. *J. Chem. Phys.* **1993**, *98*, 4128.
(228) Leggeter, S.; Tildesley, D. J. *Mol. Phys.* **1989**, *68*, 519.
(229) Trott, G. J.; Taub, H.; Hansen, F. Y.; Danner, H. R. *Chem. Phys. Lett.* **1981**, *78*, 504.
(230) Krim, J.; Suzanne, J.; Shechter, H.; Wang, R.; Taub, H. *Surf. Sci.* **1985**, *162*, 446.
(231) Newton, J. C.; Dennison, J. R.; Wang, S. K.; Wang, R.; Taub, H.; Conrad, E.; Shechter, H. *Bull. Am. Phys. Soc.* **1987**, *32*, 467.
(232) Smith, D. P. E.; Hörber, J. K. H.; Binnig, G.; Nejoh, H. *Nature* **1990**, *344*, 641.
(233) McGonigal, G. C.; Bernhardt, R. H.; Thomson, D. J. *Appl. Phys. Lett.* **1990**, *57*, 28. McGonigal, G. C.; Bernhardt, R. H.; Yeo, Y. H.; Thomson, D. J. *J. Vac. Sci. Tech. B* **1991**, *9*, 1107.
(234) Rabe, J. P.; Buchholtz, S. *Phys. Rev. Lett.* **1991**, *66*, 2096; *Science* **1991**, *253*, 424.
(235) Watel, G.; Thibaudau, F.; Cousty, J. *Surf. Sci.* **1993**, *281*, L297.
(236) Hentschke, R.; Schürman, B.; Rabe, J. *J. Chem. Phys.* **1992**, *96*, 6213.
(237) Vernov, A.; Steele, W. A. *Langmuir* **1991**, *7*, 3110; 2817.
(238) Monkenbusch, M.; Stockmeyer, R. In *Ordering in Two Dimension*; Sinha, S., Ed.; Elsevier-North Holland: New York, 1980. Monkenbusch, M.; Stockmeyer, R. *Ber. Bunsen-Ges. Phys. Chem.* **1980**, *84*, 808. Stockmeyer, R.; Stortnik, R. *Surf. Sci.* **1979**, *81*, L315.
(239) Meehan, P.; Rayment, T.; Thomas, R. K.; Bomchil, G.; White, J. W. *J. Chem. Soc., Faraday Trans. 1* **1980**, *76*, 2011.
(240) Bondi, C.; Taddei, G. *Surf. Sci.* **1988**, *203*, 587. Bondi, C.; Baglioni, P.; Taddei, G. *J. Chem. Phys.* **1985**, *96*, 277.
(241) Tabony, J.; White, J. W.; Delachaume, J. C.; Coulon, M. *Surf. Sci.* **1980**, *95*, L282.
(242) Bardi, U.; Magnanelli, S.; Rovida, G. *Langmuir* **1987**, *3*, 159. Bardi, U.; Magnanelli, S.; Rovida, G. *Surf. Sci.* **1986**, *165*, L7.
(243) Gameson, I.; Rayment, T. *Chem. Phys. Lett.* **1986**, *123*, 150.
(244) Razafitianamaharavo, A.; Convert, P.; Coulomb, J. P.; Croset, B.; Dupont-Pavlovsky, N. *J. Phys. (Paris)* **1989**, *50*, 3133.
(245) Stephens, P. W.; Huth, F. *Phys. Rev. B* **1985**, *32*, 1661.
(246) Abdelmoula, M.; Ceva, T.; Croset, B.; Dupont-Pavlovsky, N. *Surf. Sci.* **1992**, *274*, 129.
(247) Marti, C.; Ceva, T.; Croset, B.; De Beauvais, C.; Thomy, A. *J. Phys. (Paris)* **1986**, *47*, 1517.
(248) Shirazi, A. R. B.; Knorr, K. *Mol. Phys.* **1993**, *78*, 73.
(249) Lauter, H. J.; Croset, B.; Marti, C.; Thorel, P. In *Ordering in Two Dimensions*; Sinha, S., Ed.; Elsevier-North Holland: New York, 1980.
(250) Knorr, K. *Phys. Rep.* **1992**, *214*, 113.
(251) Hammond, W. R.; Mahanti, S. D. *Surf. Sci.* **1990**, *234*, 308.
(252) Suzanne, J.; Coulomb, J. P.; Bienfait, M.; Matecki, M.; Thomy, A.; Croset, B.; Marti, C. *Phys. Rev. Lett.* **1978**, *41*, 760.
(253) Morishige, K.; Kawamura, K.; Kose, A. *J. Chem. Phys.* **1990**, *93*, 5267.
(254) Morishige, K. *J. Chem. Phys.* **1992**, *97*, 2084.
(255) Herwig, K. W.; Trouw, F. R. *Phys. Rev. Lett.* **1992**, *69*, 89.
(256) Monkenbusch, M.; Lauter, H. J. *Surf. Sci.* **1987**, *191*, 547.
(257) Rowntree, P.; Scoles, G.; Xu, J. *J. Chem. Phys.* **1990**, *92*, 3853.
(258) Cheng, A.; Steele, W. A. *J. Chem. Phys.* **1990**, *92*, 3858.
(259) Gamlen, P. H.; Thomas, R. K.; Trewern, T. D.; Bomchil, G.; Harris, N.; Leslie, M.; Tabony, J.; White, J. W. *J. Chem. Soc., Faraday Trans. 1* **1979**, *75*, 1542.
(260) Nicholson, D. *Surf. Sci.* **1984**, *146*, 480.
(261) Fowler, P. W.; Hutson, J. M. *Surf. Sci.* **1986**, *165*, 289.
(262) Chung, S.; Cole, M. W. *Surf. Sci.* **1984**, *145*, 269.
(263) Harris, J.; Feibleman, P. J. *Surf. Sci.* **1982**, *115*, L133.

(264) Schmeits, M.; Lucas, A. A. *Chem. Phys. Lett.* **1975**, *35*, 391; *Surf. Sci.* **1977**, *64*, 176.
(265) Cole, M. W.; Schmeits, M. *Surf. Sci.* **1978**, *75*, 529.
(266) Ihm, G.; Cole, M. W.; Toigo, F.; Scoles, G. *J. Chem. Phys.* **1987**, *87*, 3995.
(267) Celli, V. In *Helium Atom Scattering from Surfaces*; Hulpke, E., Ed.; Springer-Verlag: Berlin, 1992.
(268) Jiang, X.-P.; Toigo, F.; Cole, M. W. *Chem. Phys. Lett.* **1983**, *101*, 159; *Surf. Sci.* **1984**, *145*, 281; **1984**, *148*, 21.
(269) Hutson, J. M.; Fowler, P. W.; Zaremba, E. *Surf. Sci.* **1986**, *175*, L775.
(270) Girard, C.; Labani, B.; Vigoureux, J. M. *Surf. Sci.* **1989**, *222*, 259.
(271) Nørskov, J. K.; Jacobsen, K. W.; Stoltze, P.; Hansen, L. B. *Surf. Sci.* **1993**, *283*, 277.
(272) Cole, M. W.; Toigo, F. *Phys. Rev. B* **1985**, *31*, 727. Frigo, A.; Toigo, F.; Cole, M. W.; Goodman, F. O. *Phys. Rev. B* **1986**, *33*, 4184. Ihm, G.; Cole, M. W.; Toigo, F.; Klein, J. R. *Phys. Rev. A* **1990**, *42*, 5244. Ihm, G.; Cole, M. W. *Langmuir* **1989**, *5*, 550; *Phys. Rev. A* **1989**, *40*, 1153.
(273) Nicholson, D. *Surf. Sci.* **1985**, *151*, 553; **1987**, *184*, 255.
(274) Klein, J. R.; Bruch, L. W.; Cole, M. W. *Surf. Sci.* **1986**, *173*, 555. Klein, J. R.; Cole, M. W. *Surf. Sci.* **1983**, *134*, 722. Chung, S.; Holter, N.; Cole, M. W. *Phys. Rev. B* **1985**, *31*, 6660; *Surf. Sci.* **1986**, *165*, 466. Kim, H.-Y.; Cole, M. W. *Phys. Rev. B* **1987**, *35*, 3990.
(275) Aziz, R. A.; Buch, U.; Jónsson, H.; Ruiz-Suárez, J.-C.; Schmidt, B.; Scoles, G.; Slaman, M. J.; Xu, J. *J. Chem. Phys.* **1989**, *91*, 6477; **1990**, *93*, 4492.
(276) Jónsson, H.; Weare, J. H. *Phys. Rev. Lett.* **1986**, *57*, 412.
(277) Kim, H.-Y.; Cole, M. W.; Toigo, F.; Nicholson, D. *Surf. Sci.* **1988**, *198*, 555. Kim, H.-Y.; Cole, M. W. *Surf. Sci.* **1988**, *194*, 257.
(278) Annett, J. *Phys. Rev. B* **1987**, *35*, 7826.
(279) Chizmeshya, A.; Zaremba, E. *Surf. Sci.* **1992**, *268*, 432.
(280) Bruch, L. W. *Surf. Sci.* **1983**, *125*, 194.
(281) Bruch, L. W.; Cohen, P. I.; Webb, M. B. *Surf. Sci.* **1976**, *59*, 1.
(282) Chiang, T.-C.; Kaindl, G.; Eastman, D. E. *Sol. State Commun.* **1982**, *41*, 661.
(283) Chesters, M. A.; Hussain, M.; Prichard, J. *Surf. Sci.* **1973**, *35*, 161.
(284) Tang, K. T.; Toennies, J. P. *Surf. Sci.* **1992**, *279*, L203.
(285) Ishi, S.; Viswanathan, B. *Thin Solid Films* **1991**, *201*, 373.
(286) Barker, J. A.; Rettner, C. T. *J. Chem. Phys.* **1992**, *97*, 5844. Bethune, D. S.; Barker, J. A.; Rettner, C. T. *J. Chem. Phys.* **1990**, *92*, 6847.
(287) Müller, J. E. *Phys. Rev. Lett.* **1990**, *65*, 3021.
(288) Tully, J. C. *Surf. Sci.* **1981**, *111*, 461. Arumainayagam, C. R.; Madix, R. J.; McMaster, M. C.; Suzawa, V. M.; Tully, J. C. *Surf. Sci.* **1990**, *226*, 180.
(289) Rejto, P.; Andersen, H. C. *J. Chem. Phys.* **1993**, *98*, 7636.
(290) Kern, K.; David, R.; Palmer, R. L.; Comsa, G. *Phys. Rev. Lett.* **1986**, *56*, 620. Poelsma, B.; Verheij, L. K.; Comsa, G. *Surf. Sci.* **1985**, *152/153*, 851. Kern, K.; David, R.; Zeppenfeld, P.; Comsa, G. *Surf. Sci.* **1988**, *195*, 453.
(291) Cassuto, A.; Ehrhardt, J. J.; Cousty, J.; Riwan, R. *Surf. Sci.* **1988**, *194*, 453.
(292) Schönhense, G.; Eyers, A.; Friess, U.; Schäfers, F.; Heinzman, U. *Phys. Rev. Lett.* **1985**, *54*, 547. Schönhense, G. *Appl. Phys. A* **1986**, *41*, 39.
(293) Black, J. E.; Janzen, A. *Phys. Rev. B* **1988**, *38*, 8494; **1989**, *39*, 6238; *Langmuir* **1989**, *5*, 558; *Surf. Sci.* **1989**, *217*, 199. Black, J. E.; Bopp, P. *Surf. Sci.* **1987**, *182*, 98; *Phys. Rev. B* **1986**, *34*, 7410.
(294) Cheng, E.; Cole, M. W.; Dupont-Roc, J.; Saam, W. F.; Treiner, J. *Rev. Mod. Phys.* **1993**, *65*, 557. Cheng, E.; Mistura, G.; Lee, H. C.; Chan, M. H. W.; Cole, M. W.; Carraro, C.; Saam, W. F.; Toigo, F. *Phys. Rev. Lett.* **1993**, *70*, 1854.
(295) Schwennicke, C.; Schimmelpfennig, J.; Pfnür, H. *Phys. Rev. B* **1993**, in press.
(296) Morishige, K.; Takami, Y.; Yokota, Y. *Phys. Rev. B* **1993**, in press.
(297) Morishige, K.; Kawai, N.; Shimizu, M. *Phys. Rev. Lett.* **1993**, in press.